CHAPTER 3

RESULTS AND DISCUSSION

3.1 Synthesis of Pentaerythritol tetrakis(6'-hydroxyhexanoate)

The retrosynthetic analysis of compound **7** could be derided from pentarythritol (**5**) and ε-caprolactone (**1**) as shown in Scheme 3.1.

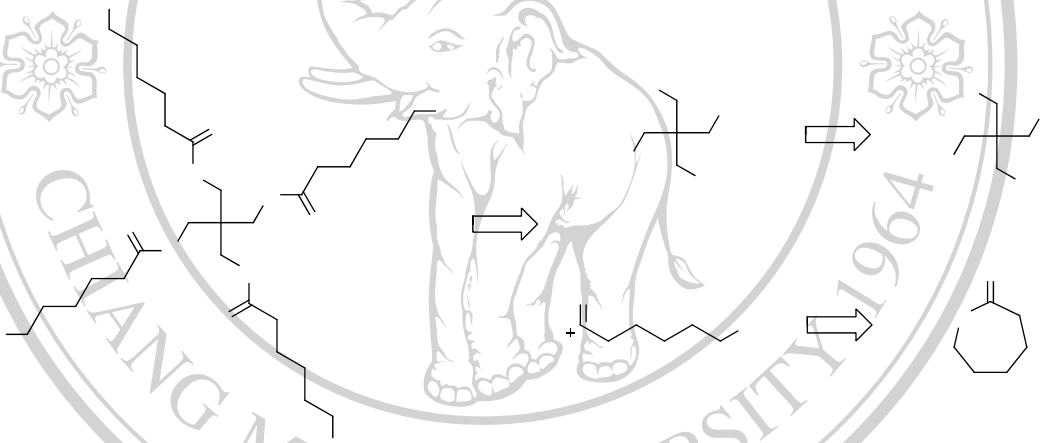

Scheme 3.1 Retrosynthesis of pentaerythritol tetrakis(6'-hydroxyhexanoate)

The star-core macroinitiator **7**, pentaerythritol tetrakis(6'-hydroxyhexanoate) could be synthesized from ε-caprolactone (**1**) as shown in Scheme 3.2, *via* transmethylation, alcohol protection, hydrolysis, esterification and deprotection respectively.

OH

OH

O

O

O

O

O

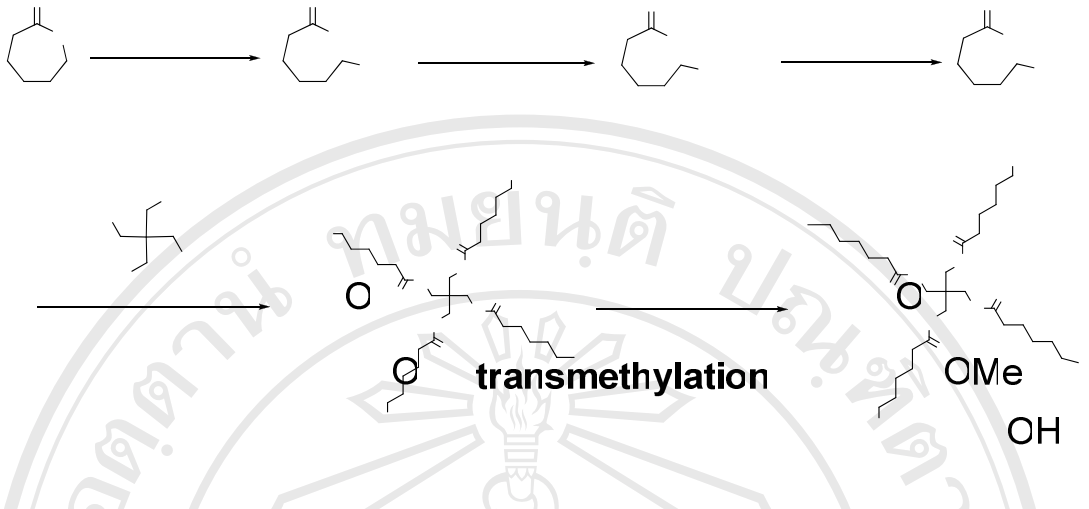

Scheme 3.2 Synthesis of pentaerythritol tetrakis(6'-hydroxyhexanoate) (**7**)

Synthesis of pentaerythritol tetrakis(6'-hydroxyhexanoate) (**7**) was started from transmethylation reaction of ε-caprolactone (**1**) as shown in Scheme 3.3. A mixture of compound **1** and conc. H_2SO_4 in excess anhydrous methanol was heated to reflux overnight. Compounds **2** in 79% yield were obtained by flash column chromatography (silica gel) using ethyl acetate (EtOAc) : hexanol = 1 : 9 as eluent.

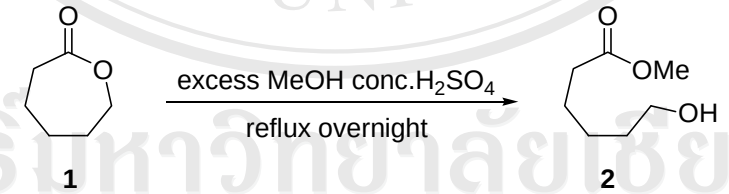

Scheme 3.3 Translation of methyl 6-hydroxyhexanoate (**2**)

Compound **2** was identified by spectroscopic techniques, ^{1}H NMR data of methyl ester of **2** appeared singlet δ at 3.68 ppm, the proton at 2-position appeared triplets δ at 2.34 ppm and the proton at 6-position appeared triplets δ at 3.66 ppm as

shown in Figure 3.1. IR data displayed broad peak of O-H stretching of hydroxyl at 3403 cm^{-1} and C=O stretching of ester at 1732 cm^{-1}.

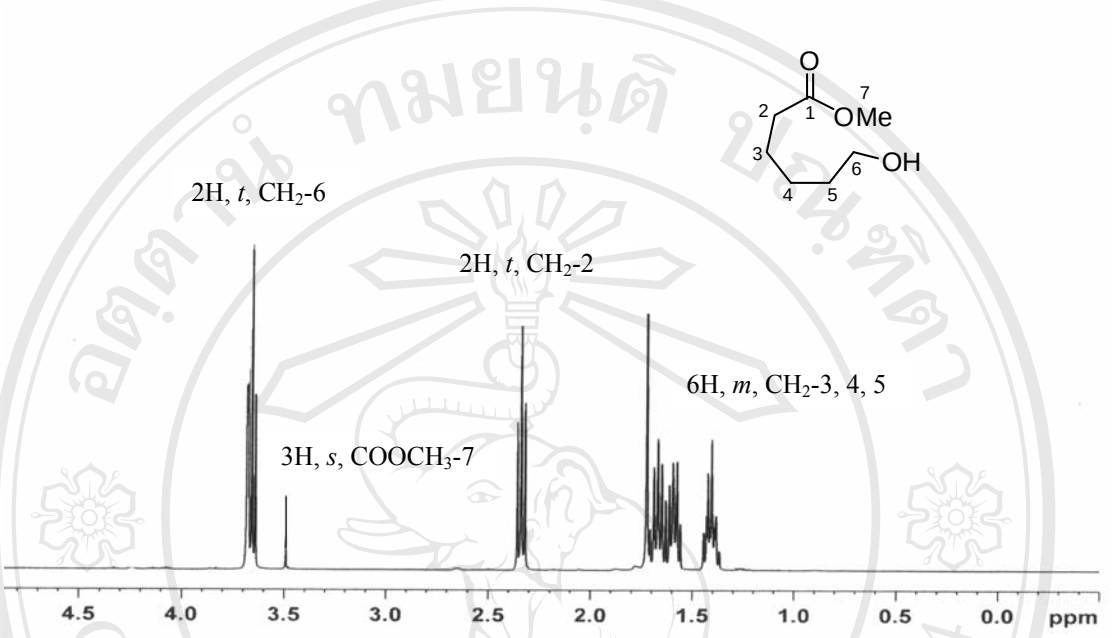

Figure 3.1 ^{1}H-NMR spectra data of compound **2**.

The protection of active hydroxyl group was success by using 3,4-dihydro-2*H*-pyran (1.5 eq.) in the $CHCl_3$ solution and present of montmorillonite K10 as a catalyst gave compound **3** as shown in Scheme 3.4.

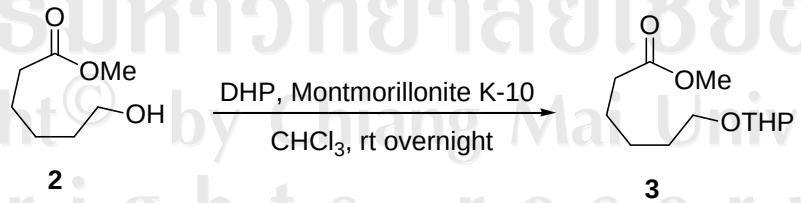

2 **3**

Scheme 3.4 Protection of alcohol by using DHP and M-K10

Compound **3** was identified by spectroscopic techniques, ^{1}H NMR data of methyl ester of **3** appeared singlet δ at 3.69 ppm and CH–O triplet δ at 4.59 ppm as shown in Figure 3.2. IR data displayed peak of C–O stretching of ether at 1074, 1035 cm^{-1} and ESI-MS data revealed 253.1416 m/z $(M + Na)^{+}$ of $C_{12}H_{22}O_4Na$.

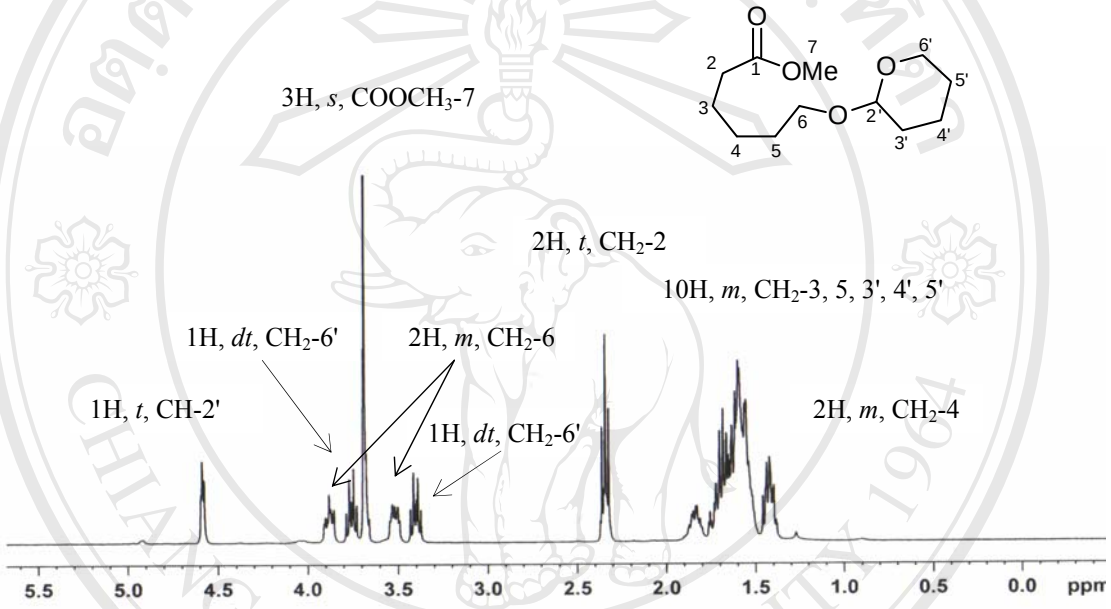

Figure 3.2 ^{1}H-NMR spectra data of compound **3**.

Subsequently, the methyl protected hydroxyl ester **3**, was hydrolyzed by NaOH to reflux in methanol and water for 1 h to give the ether acid **4** as shown in Scheme 3.5.

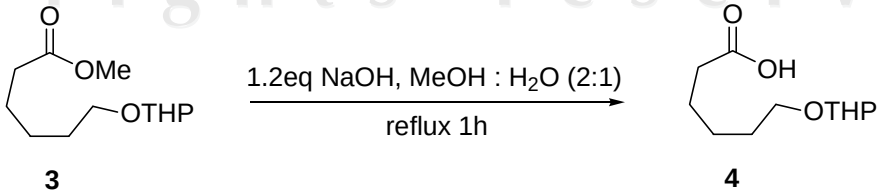

3 **4**

Scheme 3.5 hydrolysis of compound **3**

Compound **4** was identified by spectroscopic techniques, ^{1}H NMR data of CH–O at 2'-position of **4** appeared triplrts δ at 4.60 ppm, the proton at 6'-position appeared double of doublets δ at 3.41 ppm (J = 9.63, 6.48 Hz), 3.76 ppm (J = 9.62, 6.71 Hz) and the proton at 6-position appeared multiplets δ at 3.52, 3.88 ppm as shown in Figure 3.3. IR data displayed peak of C=O stretching of carboxylic acid at 1711 cm^{-1} and ESI-MS data revealed 239.1259 m/z $(M + Na)^{+}$ of $C_{11}H_{20}O_4Na$.

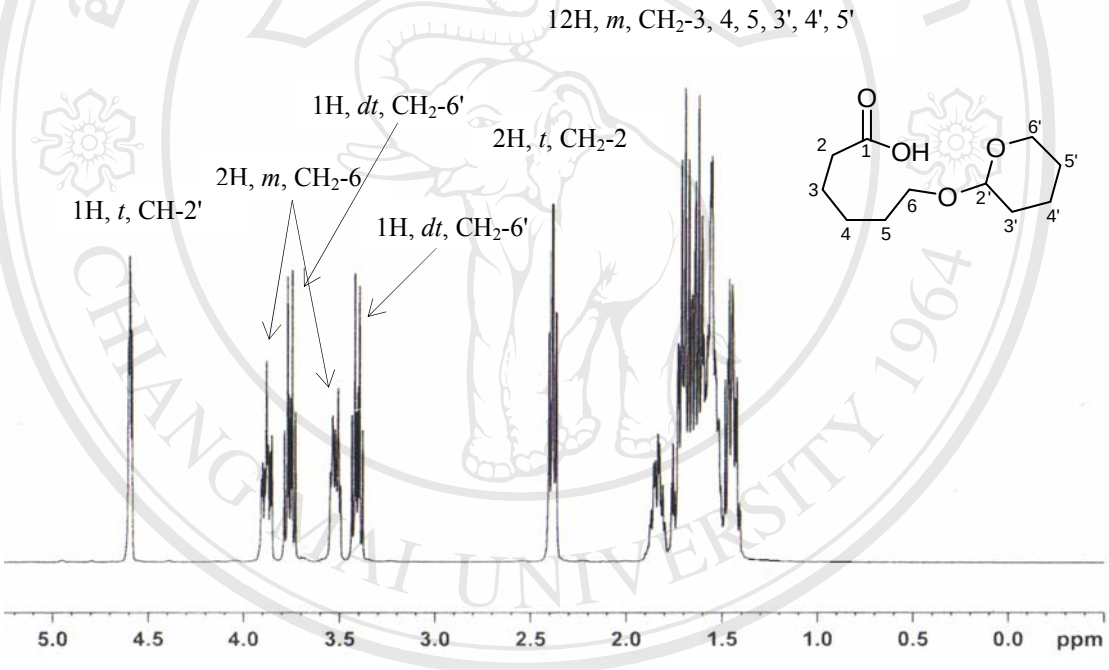

Figure 3.3 ^{1}H-NMR spectra data of compound **4**.

Final step, compound **4** reacted with pentaerythritol (**5**) in the presence of *N,N'*-dicyclohexylcarbodiimide (DCC) and 4-dimethlaminopyridine (DMAP) to yield compound **6** and then the THP group of **6** was removed by stirring with montmorillonite K-10 in methanol to yield the star-core macroinitiator (**7**) as shown in Scheme 3.6.

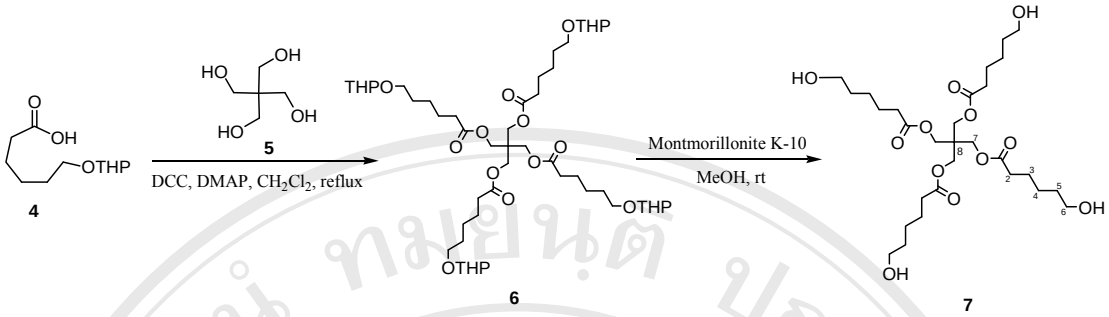

Scheme 3.6 Esterification and deprotection of compound **7**

The final product **7** was identified by spectroscopic techniques, ^{1}H NMR spectra data shown the proton at 7-position appeared singlet δ at 4.10 ppm, the proton at 6-position appeared triplets δ at 3.61 ppm (J = 6.32 Hz) and the proton at 2-position appeared triplets δ at 2.35 ppm as shown in Figure 3.4.

The IR spectrum shown absorption peaks at 1153 cm^{-1} of C-O stretching of ester, at 1407 cm^{-1} of CH_2 bending, at 1747 cm^{-1} of C=O stretching of ester, 2946 and 2871 cm^{-1} of CH_2 stretching and at 3381 cm^{-1} of O–H stretching of alcohol as shown in Figure 3.5. ESI-MS data revealed 615.3356 m/z $(M + Na)^+$ of $C_{29}H_{52}O_{12}Na$.

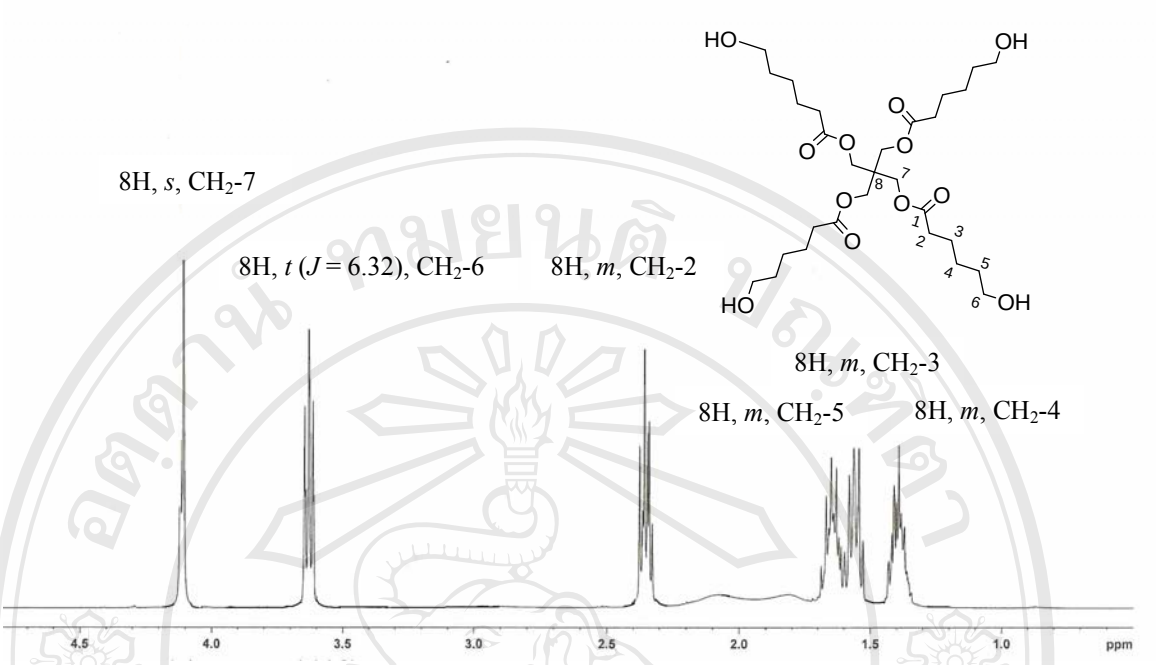

Figure 3.4 ^{1}H-NMR spectra data of compound **7**.

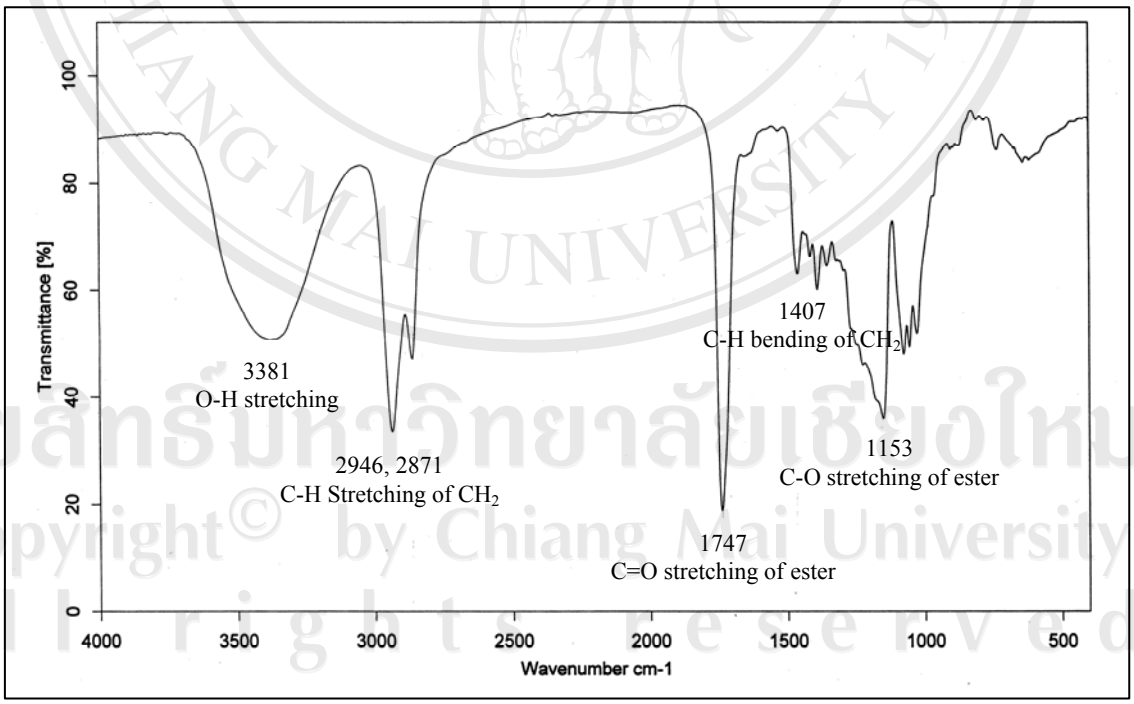

Figure 3.5 IR data of compound **7**.

3.2 Synthesis of Low Molecular Weight PCL Model Compounds with Different Molecular Architectures

Low molecular weight PCL model compounds with different molecular architectures were synthesized by ROP of ε-caprolactone at 120ºC for 48 hours using 0.1 mole % $SnOct_2$ as a catalyst and 4 mole % of 1-hexanol, PTOL and pentaerythritol tetrakis(6'-hydroxyhexanoate) as initiators. The structure of the PCLs depends on the functional initiating cores. Monofunctional alcohol (1-hexanol) yielded linear PCL (PCL_1-hexanol), while multifunctional alcohols (PTOL) and multifunctional pentaerythritol tetrakis(6'-hydroxyhexanoate) macroinitiator yielded star-shaped PCLs (PCL_PTOL and PCL_macroinitiator respectively) as shown in Figure 3.6 (a-c). The route of synthesis in this study was the core-first method where polymer chains were grown directly from a functional core.

Relatively high amount of initiator (4% by mole monomer) was used to obtain low molecular weight PCLs as model compounds in order to confirm the structure and evaluate the influence of short-chain architecture on the properties. The structures and properties of the resulting PCL oligomers were characterized by GPC, dilute-solution viscometry, ^{1}H-NMR, DSC and TG analysis. All results are summarized in Table 3.1 and the details will be described in the following sections. The physical appearance of PCL_1-hexanol was white solids. In contrast, PCL_PTOL and PCL_macroinitiator were sticky solid. The yields of purified PCLs model compounds were quite low (65-88%) because of the high alcohol concentration used.

(a)

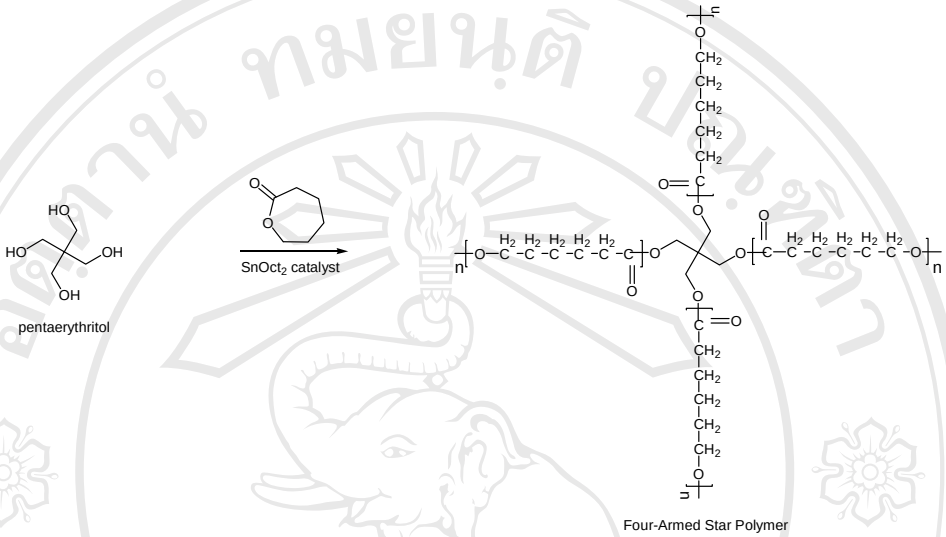

(b)

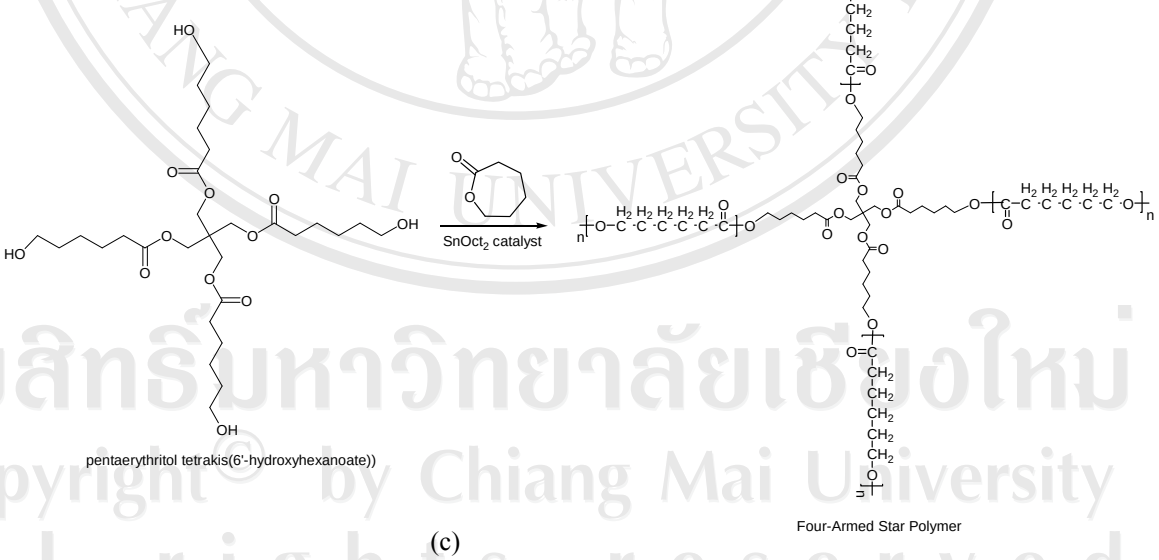

(c)

Figure 3.6 Polymerization of *ε*-caprolactone using 0.1 mole % $SnOct_2$ as a catalyst and 4 mole% of (a) 1-hexanol (b) PTOL and (c) pentaerythritol tetrakis(6'-hydroxyhexanoate) as initiators at 120ºC for 48 hours**.**

Table 3.1 The results of low molecular weight PCL model compound with different molecular architectures.

Polymer	**PCL_1-hexanol**	**PCL_PTOL**	**PCL_macroinitiator**
Amount of Polymer (g)	2	2	2
Catalyst (mole%)	$SnOct_2$ (0.1)	$SnOct_2$ (0.1)	$SnOct_2$ (0.1)
Initiator (mole%)	1-hexanol	PTOL	Macroinitator
Monomer : Initiator (mole%)	100 : 3.94	100 : 3.94	100 : 4.74
Temperature (ºC) ***and Time*** (hr)	120°C, 48 hr	120°C, 48 hr	120°C, 48 hr
% yield (purified)	88.5	65.0	74.0
Physical Appearance (crude)	white solid	colorless liquid	colorless liquid
Physical Appearance (purified)	white solid	sticky solid	sticky solid
Molecular weight (g $mole^{-1}$)			
$\overline{M}_{n,theory}$	2,956	3,033	2,970
GPC			
$\overline{M}_n$	1,662	1,718	894
$\overline{M}_v$	8,274	5,330	3,555
$\overline{M}_w$	5,213	3,884	2,381
Dilute-Solution Viscometry			
$[\eta]$ in THF at 30ºC (dl/g)	0.11	0.10	0.09
$\overline{M}_v$	4,572	4,319	3,593
$g^{1/2}$ *	-	0.80	0.80
g' **	-	0.91	0.82
$g^{1/2}/g'$ ***	-	0.88	0.98
^{1}H-NMR			
Average DP_n/Arm, $_{NMR}$	27.8	7.9	7.6
Average DP_n/Arm, $_{Theory}$	25.0	6.3	6.3
Number of initiating OH, $_{NMR}$	0.9	3.2	3.3
Number of initiating OH, $_{Theory}$	1.0	4.0	4.0
$\overline{M}_{n,NMR}$	3,271	3,734	3,606

Table 3.1 The results of low molecular weight PCL model compounds with different molecular architectures (continued).

Polymer	**PCL_1-hexanol**		**PCL_PTOL**		**PCL_macroinitiator**	
Thermal Properties						
DSC	1st run	2nd run	1st run	2nd run	1st run	2nd run
T_m, onset (ºC)	53.7	51.4	36.3	32.4	34.5	-
T_m, Peak (ºC)	59.7	55.0	44.5	35.8	40.0	-
Heat of Fusion (J/g)	108.3	94.8	59.3	60.0	34.4	-
Degree of Crystallinity (%)	80.2	70.2	43.9	44.4	25.4	-
TGA						
$T_{d,\ 10\%}$ (ºC)	340		349		341	
$T_{d,\ 50\%}$ (ºC)	372		384		384	
$T_{d,\ range}$ (ºC)	157-545		116-554		103-549	

Note * The ratio of mean-square radius of gyration of a star-shaped polymer with the number of arms (*f*)

** The ratios of intrinsic viscosities of star-shaped polymer to that of linear polymer

*** For a star-shaped polymer with perfect arm structure, there will be an important relationship $g^{1/2}/g' = 1.0$

3.2.1 Molecular Weight Determination of PCL Model Compounds by GPC and Dilute-Solution Viscometry

In this study, the average molecular weights of low molecular weight PCL model compounds were determined by GPC. Typical GPC curves of the purified PCL model compounds are shown in Figure 3.7 and the various average molecular

weights ($\overline{M}_n$, $\overline{M}_v$ and $\overline{M}_w$) for all samples are compared with $\overline{M}_n$'s theoretical values in Table 3.1.

From GPC results, the molecular weight of purified linear and star-shaped PCL model compounds ($\overline{M}_{n,GPC}$ ≈ 900-1,700) were controlled by using the ratio 100:4 mole% of monomer to initiator. As expected, the low molecular weight PCL was achieved with using the high concentration of initiator, consistent with reports from Dong *et al.* [50, 51] and Thapsukhon [59]. The result indicates that hydroxyl-containing compounds are real initiator, which can stoichiometrically control the molecular weight of the polymer. The $SnOct_2$ acted only as a catalyst, increasing the polymerization rate but having no effect on the molecular weight. However, controlled polymerization has been achieved when using very dry systems with a controlled amount of a hydroxyl-containing compound.

The GPC curve presented unimodal molecular weight distribution (MWD), which suggests that no mixture of star-shaped and linear is formed. The theoretical number-average molecular weight ($\overline{M}_{n,theory}$) were calculated from $\overline{M}_{n,theory}$ = $MW_{initiator}$ + (n × MW of ε-caprolactone), where n = number of repeating unit (mole of ε-caprolactone / mole of initiator).

Sample Calculation: for PCL_1-hexanol

$$\text{Theoretical number - average molecular weight} = 102.18 + (\frac{100x114.14}{4})$$

$$= 2956 \text{ g mole}^{-1}$$

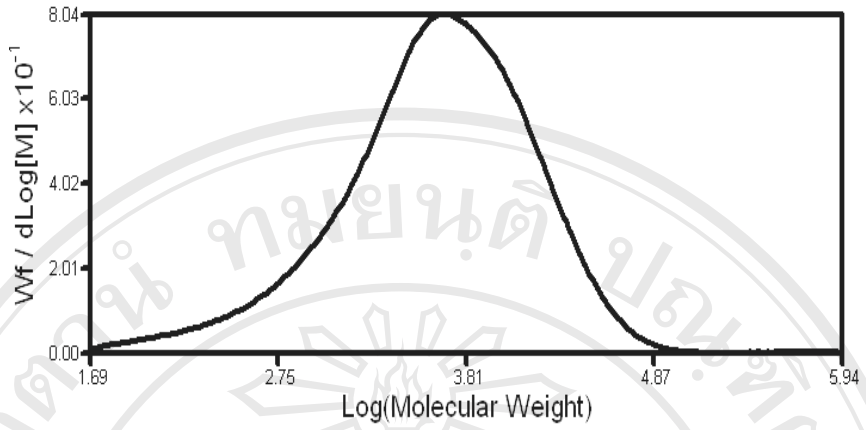

(a)

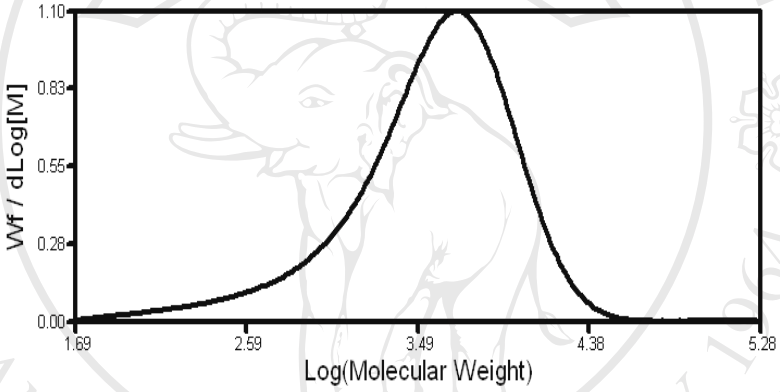

(b)

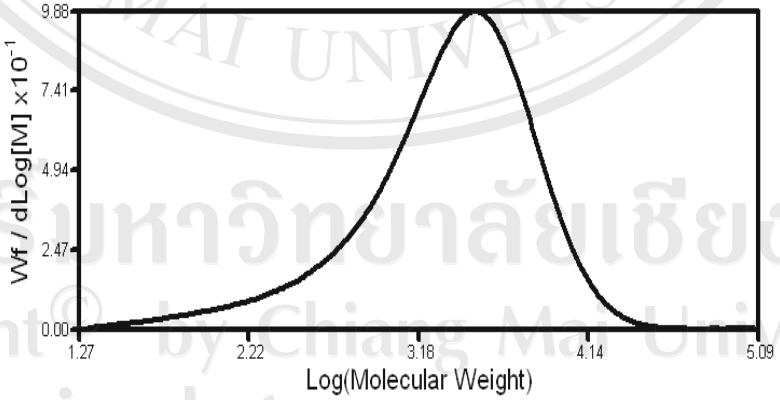

(c)

Figure 3.7 GPC curves of low molecular weight purified PCL model compounds; (a) PCL_1-hexanol (b) PCL_PTOL and (c) PCL_macroinitiator.

The calculated number average molecular weight ($\overline{M}_{n,theory}$) using the following equations assuming that all of initiating molecules acted and were incorporated in the polymers. Bearing in mind that variation in the number of arms was accomplished by using different initiating core initiator and the arm lengths were controlled to get the same molecular weight oligomers by controlling monomer to initiator molar ratio in this study.

The $\overline{M}_{n,GPC}$ values of all linear and star-shaped PCLs from GPC results are lower than the theoretical values that calculated from the monomer to initiator ratio assuming hydroxyl initiation as compared in Table 3.1. This indicates that initiation by another species has also occurred. However, the $\overline{M}_n$ values of star-shaped PCL_macroinitiator from GPC result ($\overline{M}_{n,GPC}$ = 894) was not close to the theoretical value ($\overline{M}_{n,theory}$ = 2970), which could be described to the unique molecular structure of star-shaped PCL. The GPC analysis always underestimates the molecular weight star-shaped polymers because it has smaller hydrodynamic volume than that of linear polystyrene having the same molecular weight. For star-shape polymers, the GPC technique is not the appropriate method to determine the molecular weight. [54]

Viscosities of the synthesized linear and star-shaped PCLs oligomers were measured at 30.0ºC in THF solution. Under a series of PCL concentrations, reduced viscosities (η_{red}) and inherent viscosities (η_{inh}) were measured and evaluated. Furthermore, intrinsic viscosity, [η] was estimated via the extrapolation of the η_{red} and η_{inh} versus polymer concentration plot and the results are shown in Table 3.2.

The viscosity-average molecular weights ($\overline{M}_v$) values of the low molecular weight PCLs were calculated from Mark-Houwink-Sakurada Equation; $[\eta] = K\overline{M}_v^{\,a}$, where *K* and *a* are the characterization parameters predominantly determined by the combination of polymer and solvent at constant temperature. An example of the type of flow-time data obtained, derived viscosity parameters, and reduced/inherent viscosity-concentration graphs are shown in Table 3.2 and Figure 3.8. The double extrapolation of the 2 graphs in Figure 3.8 to their common intercept at zero concentration (c = 0) gives the value of the intrinsic viscosity, [η], from which the value of $\overline{M}_v$ is calculated as follows:

Sample Calculation of $\overline{M}_v$: for PCL_macroinitiator

From Figure 3.8 (c)

$$[\eta] = (\eta_{red})_{c=o} = (\eta_{inh})_{c=o} = 0.0902 \text{ dl/g}$$

When this value of [η] is substituted into the Mark-Houwink-Sakurada Equation for PCL in THF as solvent at 30ºC [66] of:

$$[\eta] = 1.40 \times 10^{-4}\ \overline{M}_v^{\,0.79} \text{ dl/g}$$

it yields $0.0902 = 1.40 \times 10^{-4}\ \overline{M}_v^{\,0.79}$

$$\overline{M}_v = 3{,}593$$

From the viscosities and $\overline{M}_v$ values results, it was found that in dilute solution, low molecular weight star-shaped PCLs exhibited slightly lower intrinsic viscosity than linear PCL, indicating the expected star-shaped structure. It is due to the star-shaped has a higher segment density within the distance of its radius of gyration and lower hydrodynamic volume than linear polymers.

Table 3.2 Dilute-solution viscometry data of low molecular weight PCL_ macroinitiator using THF as solvent at 30ºC.

Concentration (g/dl)	Flow-Time* (second)	η_{rel}	η_{sp}	η_{red} (dl/g)	η_{inh} (dl/g)
solvent	120.01	-	-	-	-
0.2044	122.49	1.0207	0.0207	0.1011	0.1001
0.4268	125.81	1.0483	0.0483	0.1132	0.1106
0.6000	128.86	1.0738	0.0738	0.1230	0.1186
0.8004	133.00	1.1082	0.1082	0.1352	0.1284
1.0008	137.54	1.1461	0.1461	0.1460	0.1362

* average of at least 3 readings which agree to within ±0.2% of this average value

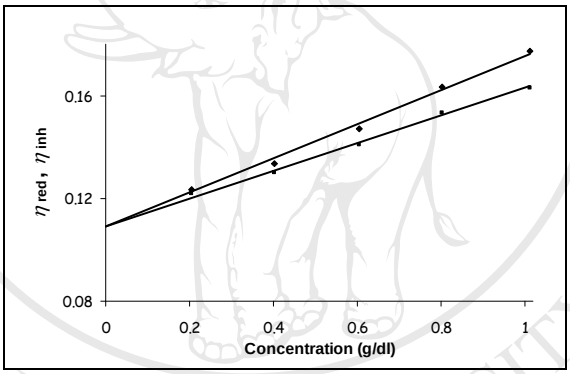

(a)

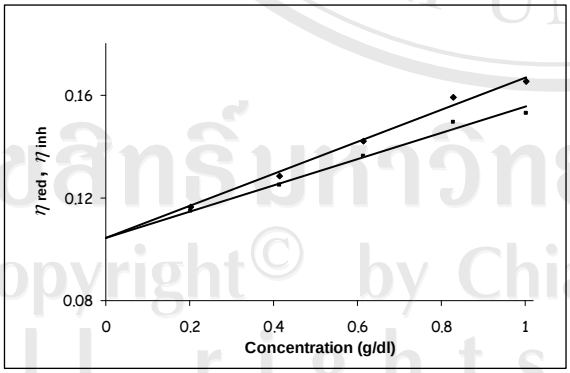

(b)

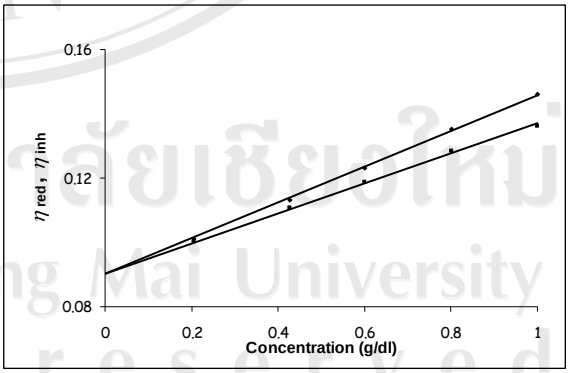

(c)

Figure 3.8 Reduced (η_{red}) and inherent (η_{inh}) viscosity-concentration plots of low molecular weight; (a) PCL_1-hexanol, (b) PCL_PTOL and (c) PCL_macroinitiator (♦ η_{red} and ■ η_{inh})

The fine structures of the synthesized star-shaped PCLs could be estimated by comparing the mean square radius of gyration and intrinsic viscosities with linear polymer. [67-69] Degree of branching of star polymer can be estimated by comparing the mean-square radii with linear polymer. The equation (3.1) provided a mean-square radius of gyration ($g^{1/2}$) of a star-shaped polymer with the number of arms (f).

$$g^{1/2} = \frac{6f}{(f+1)(f+2)} \qquad \text{…….. (3.1)}$$

The ratios of intrinsic viscosities of star-shaped PCLs to that of linear PCL (g') bearing similar absolute molecular weight could be experimentally estimated in accordance to equation 3.2

$$g' = [\eta]_{star}/[\eta]_{linear} = K_{star}M_w^{\ a}(\text{star})/K_{linear}M_w^{\ a}(\text{linear}) \qquad \text{…….. (3.2)}$$

where K and a represent Mark-Houwink constants.

For a star-shaped polymer with perfect arm structure, there will be an important relationship of $g^{1/2} = g'$ or $g^{1/2}/g' = 1.0$ as proposed by Zimm and Kilb. [69] From Table 3.1 summarized the calculated values of $g^{1/2}/g'$ for the star-shaped PCLs prepared with PTOL and macroinitiator. It could be seen that the $g^{1/2}/g'$ value of star-shaped PCL_macroinitiator (0.98) was very close to 1.0 for an ideal star-shaped polymer with perfect arm architecture. [69] Deviations from this relationship for PCL_PTOL (0.88) would point to contamination of the system, e.g. with linear chains.

GPC and dilute-solution viscosity analysis are not the appropriate method to determine the molecular weight for star-shaped polymer. Since it has the smaller hydrodynamic volume than that of linear polystyrene having the same molecular weight, the GPC analysis always underestimates the molecular weight of star-shaped polymers. However, simultaneous measurement of light scattering intensity and concentration allows direct determination of the weight molecular weight of the eluted fraction, without calibration using the standard. To identify the chain branching, GPC can be coupled with viscometer or laser light scattering detectors, such as low-angle laser light scattering (LALLS) or multi-angle laser light scattering (MALLS) detectors. For polymer with low molar mass, light scattering may suffer from a lack of sensitivity; hence, a viscometer coupled with GPC constituted an interesting alternative. [70]

3.2.2 Structural Analysis and Molecular Weight Determination of PCL Model Compounds by ^{1}H-NMR Spectroscopy

The structure of the low molecular weight PCL model compounds with different molecular architectures were characterized by ^{1}H-NMR. The ^{1}H-NMR spectra of PCLs in deuterated chloroform solutions were recorded using a Bruker Avace 400 MHz NMR spectrometer with tetramethylsilane (TMS) as internal standard at room temperature. The spectra of purified PCLs are shown in Figure 3.9. The summarized interpretations from the proton assignments of corresponding chemical shift and peak area integration are given in Table 3.3.

The low molecular weight PCLs spectra show characteristic peaks of CL unit in agreement with previous study. [50] The characteristic peak of monomer unit and initiators were similarly assigned as shown in Figure 3.9. The CH_2-OH methylene proton signal (hydroxyl at end chain, (g)) of the PCL arms were found in all samples at 3.55-3.63 ppm and the results confirmed that PCL was terminated by hydroxyl end groups [71]. The appearance of CH_2-O (a) of PTOL and PTOL_macroinitiator initiated polymerization proves that these two initiators participated in the polymerization. However, this signal in 1-hexanol initiated polymerization was not found owing to the overlapping of the CH_2-O (f) peak, the reason for this is might be both CH_2-O (a) and CH_2-O (f) have almost same surrounding protons. The methyl groups (h) of 1-hexanol initiated polymer were also found except PTOL and PTOL _macroinitiator that have no methyl group in it structure. From ^{1}H-NMR results, linear and star-shaped PCLs with hydroxyl end groups were successfully synthesized from homopolymerization of CL with different number of hydroxyl group as initiator.

The molecular weight determinate by ^{1}H-NMR spectroscopy was calculated from the integration ratio the methylene protons in the repeating unit and the methylene proton in the terminal unit. It was found that the number average molecular weight determined by ^{1}H-NMR was close to the theoretical values as compared in Table 3.1. However, the average molecular weight calculated from ^{1}H-NMR was higher than those determined by GPC. ^{1}H-NMR was used to calculate the average number of hydroxyl groups in the initiator that participate in the initiation. The initiation activity was estimated indirectly by comparing theoretical with average degree of polymerization per arm (DP_n/arm) determined by ^{1}H-NMR. All low molecular weight PCLs were analyzed and the results are shown in Table 3.4.

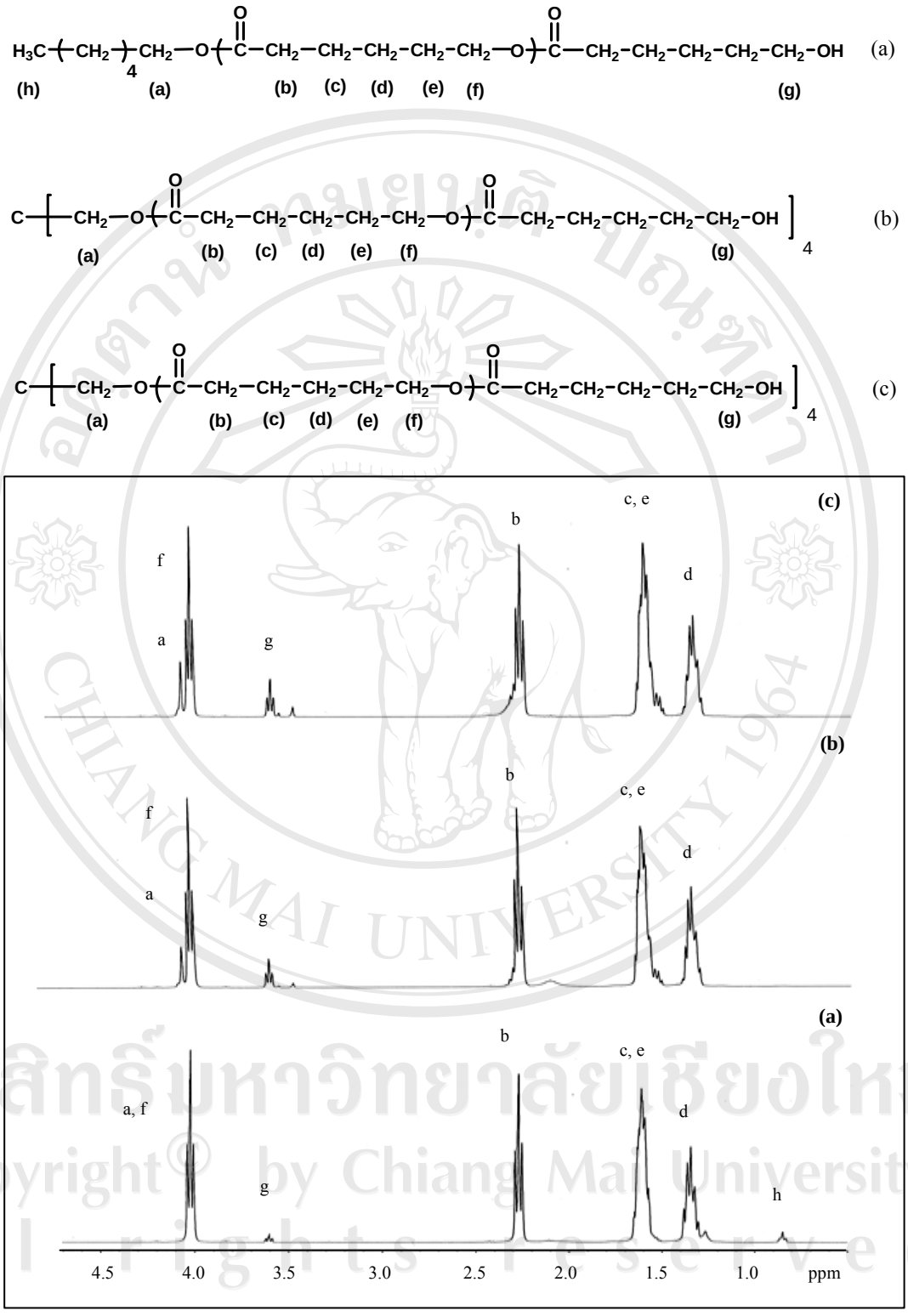

Figure 3.9 ^{1}H-NMR spectrum of low molecular weight crude PCLs; (a) PCL_1-hexanol (b) PCL-PTOL and (c) PCL-macroinitiator recorded in $CDCl_3$.

Table 3.3 Proton assignments and corresponding chemical shift ranges for the various resonance peaks in the ^{1}H-NMR spectra of the linear and star-shaped low molecular weight purified PCL model compounds.

Proton Assignment	Chemical Shift Range, δ (ppm)		
	PCL_1-hexanol	PCL_PTOL	PCL_macroinitiator
a	-	4.21-4.29	4.07-4.20
f	4.00-4.20	4.01-4.29	4.00-4.07
g	3.59-3.63	3.60-3.63	3.55-3.61
b	2.25-2.29	2.26-2.34	2.25-2.45
c, e	1.60-1.65	1.52-1.66	1.51-1.65
d	1.23-1.39	1.32-1.41	1.30-1.47
h	0.82-0.88	-	-

Table 3.4 Proton assignments and corresponding peak area integrations for the various resonance peaks in the ^{1}H-NMR spectra of the linear and star-shaped low molecular weight purified PCLs model compounds.

Proton Assignment	Peak Area Integration		
	PCL_1-hexanol	PCL_PTOL	PCL_macroinitiator
a	-	-	-
f	2.00	2.00	2.00
g	0.07	0.26	0.31
b	1.99	2.03	2.41
c, e	4.07	4.10	4.07
d	2.25	2.05	2.06
h	0.1	-	-

Average DP_n/arm of PCLs were calculated by comparing the peak integrals of chain methylene protons (Figure 3.9, (b) = 2.25-2.45 ppm) with those of methylene protons next to the terminal hydroxyl group (Figure 3.9, (g) = 3.55-3.63 ppm). This gives the average DP_n/arm in ε-caprolactone unit and, as presented in equation (3.3).

$$Average\,DP_n/arm = \frac{peak\ integral\ of\ protons\ at\ (b)}{peak\ integral\ of\ protons\ at\ (g)} \quad \text{…….. (3.3)}$$

From Table 3.4, the average DP_n/arm calculated from ^{1}H-NMR were slightly greater than the theoretical values. Probably, the difference between the calculation and theoretical values is due to the lower initiation activity of the added arm in initiator.

The number average molecular weight determined by ^{1}H-NMR spectroscopy was calculated from equation (3.4).

$$\overline{M}_{n,NMR} = MW_{initiator} + (MW\ of\ \varepsilon - caprolactone \times DP_n \times arm\ number) \quad \text{…….. (3.4)}$$

It was found that the number average molecular weight determined by ^{1}H-NMR ($\overline{M}_{n,NMR}$) was slightly higher than the theoretical values ($\overline{M}_{n,theory}$) as compared in Table 3.1. The $\overline{M}_n$ showed an order as, $\overline{M}_{n,NMR} > \overline{M}_{n,theory} > \overline{M}_{n,GPC}$.

However, GPC analysis is not the appropriate method to determine the molecular weight for star-shaped polymer. Since it has the smaller hydrodynamic volume than that of linear polystyrene having the same molecular weight, the GPC analysis always underestimates the molecular weight of star-shaped polymers. The values given by GPC are affected not by the size of the molecule but also the structure of the molecule.

The average number of hydroxyl groups in the initiator that take part in the polymerization process was determined by comparing theoretical average DP_n/arm with the average DP_n/arm determined by ^{1}H-NMR as shown in equation (3.5).

$$Number\ of\ initiating-OH = \frac{theoretical\ average\ DP_n/arm}{average\ DP_n/arm\ determined\ by\ ^1H-NMR} \times functionality \quad \ldots\ldots\ (3.5)$$

As we assumed, 1-hexanol initiating the growth of ε-caprolactone chains from one end. For example, purified PCL_1-hexanol had a theoretical average DP_n/arm of 25.0 CL units, whereas the average DP_n/arm determined by ^{1}H-NMR was 27.8. The result corresponds to value of 0.9 as the average number of hydroxyl groups initiating polymerization. As the results in Table 3.4, indicated that the linear and star-shaped PCL oligomers were successfully synthesized.

3.2.3 Thermal Characterization of PCL Model Compounds by DSC

The data in Table 3.1 compared the melting and crystallization behaviors of low molecular weight linear and star-shaped PCL model compounds synthesized using $SnOct_2$ as catalyst and different number of hydroxyl group (1- and 4-OH) initiators. The DSC thermograms of PCL model compounds are shown in Figures 3.10-3.11. The degree of crystallinity (X_c) of PCLs was determined from the enthalpy of melting using equation (3.6):

$$X_c(\%) = \frac{\Delta H_m}{\Delta H_m^{\circ}} \times 100 \quad \ldots\ldots\ (3.6)$$

where ΔH_m is the apparent enthalpy of melting of each sample and ΔH_m° is the extrapolated value of enthalpy corresponding to the melting of a 100% crystalline PCL, 135.0 J g^{-1} [72].

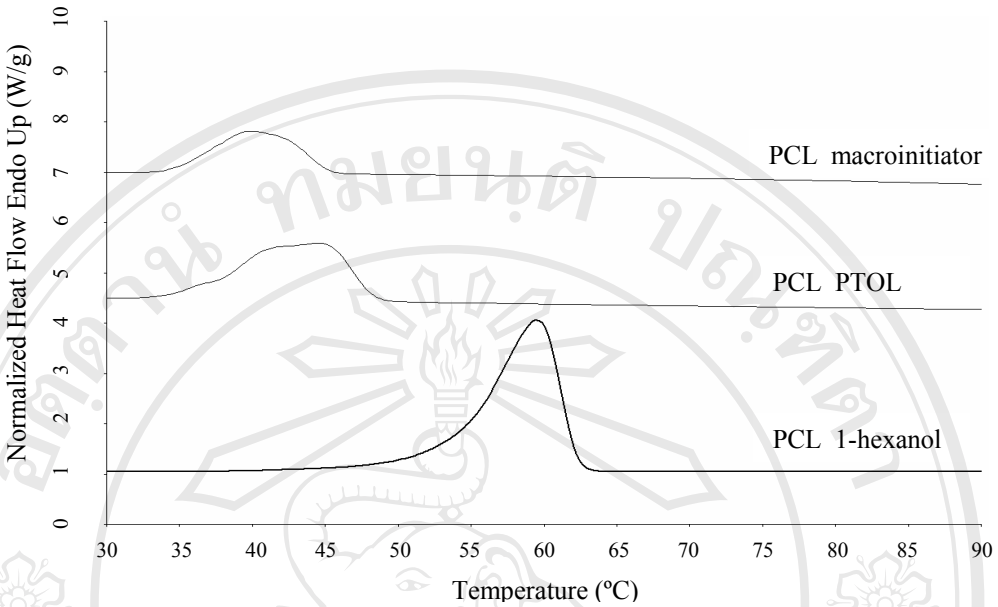

Figure 3.10 Comparison of the DSC thermograms first run of linear and star-shaped low molecular weight PCLs model compounds.

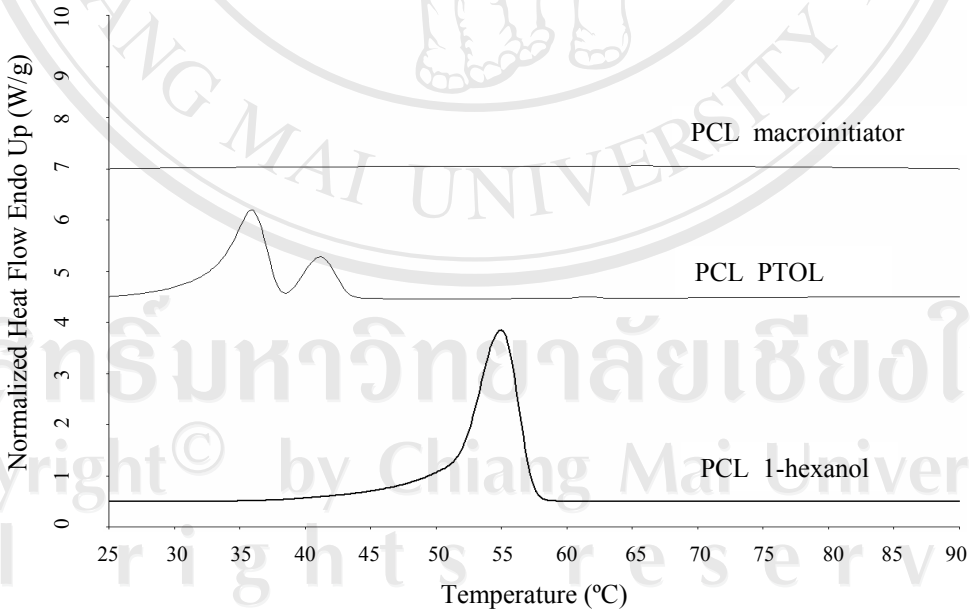

Figure 3.11 Comparison of the DSC thermograms second run of linear and star-shaped low molecular weight PCLs model compounds.

It was found that the melting temperatures (T_m) and degree of crystallinity of star-shaped PCLs (PCL_PTOL and PCL_maroinitiator) are all lower than that of linear (PCL_1-hexanol). The thermal properties will affected when branching points are introduced into the polymer. The reduction in melting point with branching is attributed to shorter chain length and the increase in the number of free chain ends, which disrupts the orderly fold pattern of the crystal and less compactly packed volume in the solution. In the second run, PCL_macroinitiator did not show any T_m because of it is very short chain length leaded to the amorphous structure. However, PCL_PTOL showed some crystallinity due to imperfect star-shape.

From Figure 3.11, PCL_PTOL, the initially existing shoulder in the first run becomes into two peaks in the second run, which could be due to the two different molecular weight distributions within the oligomeric range and probably in different spherulite morphology and size. [73] In addition, the degree of crystallinity value determined in the first heating run was apparently higher than the degree of crystallinity determined in second run heating run. This indicated that the thermal history has obvious effect on the degree of crystallinity of semicrytalline PCLs.

3.2.4 Thermal Characterization of PCL Model Compounds by TGA

The dynamic (non-isothermal) TG thermograms of the linear and star-shaped low molecular weight PCLs are shown in Figure 3.12. In each case, a heating rate of 20ºC/min was used under an inert nitrogen atmosphere. In terms of "initial" ($T_{d,\ 10\%}$), "half" decomposition ($T_{d,\ 50\%}$) and temperature degradation ranges ($T_{d,\ range}$) which the weight losses occurred were compared in Table 3.1. From TG thermograms, it was found that all PCLs model compounds showed a pattern consisting only one stage

degradation which could be ascribed to the homogeneous polymer products from the polymerization.

As depicted in Table 3.1, the values of $T_{initial}$ of PCL_1-hexanol is 157°C, whereas the corresponding values of $T_{initial}$ of PCL_PTOL and PCL_macroinitiator are 116 and 103°C, respectively. Star-shaped PCLs start to degrade at lower temperature than linear PCL. The result suggests that star-shaped PCLs significantly decrease the thermal stability of low molecular weight PCLs. It is reasonable that star-shaped PCLs, equal to higher end group concentration, show higher probability of chain cleavage and subsequently more readily undergo pyrolysis reaction. It has been generally accepted that the thermal degradation of different molecular architecture of PCLs was triggered by the participation of the end-capped hydroxyl groups. [83]

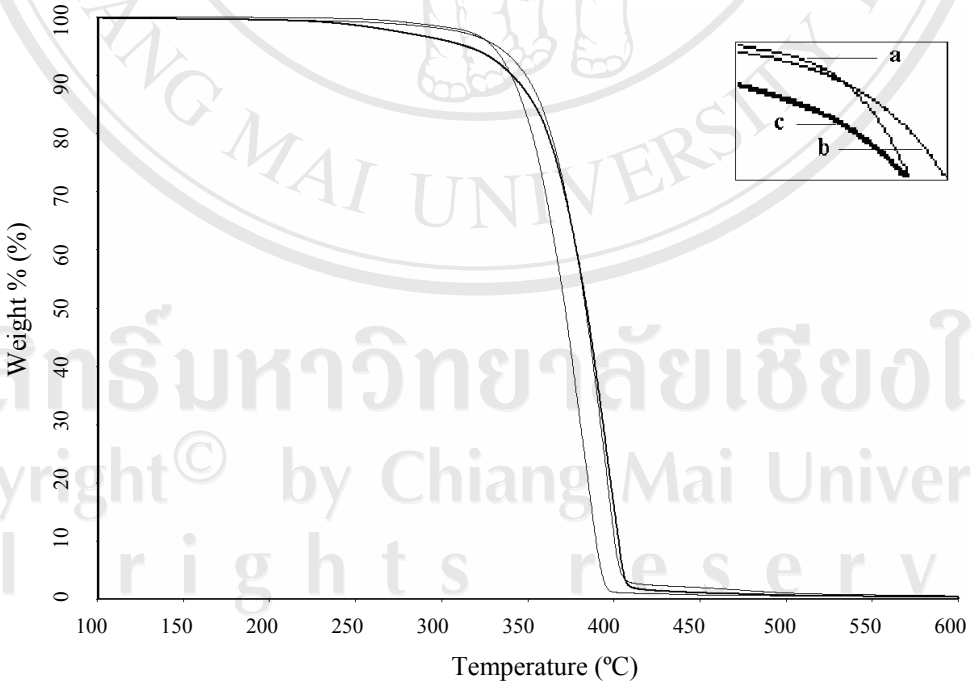

Figure 3.12 Comparison of the TG thermograms of PCL model compounds;

(a) PCL_1-hexanol, (b) PCL_PTOL and (C) PCL_macroinitiator.

3.3 Synthesis and Characterization of High Molecular Weight PCL with Different Molecular Architectures

The ROP of high molecular weight PCLs homopolymers were prepared using 0.05 mole % initiator and 0.1 mole% $SnOct_2$ as catalyst at 120ºC for 72 hours. The structure of the polymer depends on the alcohol used. Monofunctional alcohol (1-hexanol) yielded linear PCL (PCL_1-hexanol), while multifunctional alcohols (PTOL) and multifunctional pentaerythritol tetrakis(6'-hydroxyhexanoate) macroinitiator yielded star-shaped PCLs (PCL_PTOL and PCL_macroinitiator respectively) as shown in Figure 3.6 (a-c). The polymer molecular weight was fixed by controlling monomer to hydroxyl group molar ratio.

Relatively low amount of initiator (0.05% by mole monomer) was used to obtain high molecular weight PCLs in order to confirm the structure and evaluate the influence of long-chain architecture on the properties. The structures and properties of the resulting PCLs were characterized as fully as possible in order to underlying the molecular architecture-properties relationships by combination of techniques: molecular weight determination by GPC and dilute-solution viscometry, thermal transition by DSC, thermal decomposition and stability by TGA, mechanical properties by tensile testing and rheological properties by melt rheology measurements. Also, the "*in vitro*" hydrolytic biodegradability of the films was studied as an indication of their potential use in biomedical applications.

The physical appearances of all crude and purified PCLs were white solid with high % yields (97-98%). All results are summarized in Table 3.5 and the details will be described in the following sections.

Table 3.5 The results of high molecular weight PCL with different molecular architectures.

Polymer	**PCL_1-hexanol**		**PCL_PTOL**		**PCL_macroinitiator**	
Catalyst (mole %)	$SnOct_2$ (0.1)		$SnOct_2$ (0.1)		$SnOct_2$ (0.1)	
Initiator (mole %)	1-hexanol		PTOL		Macroinitiator	
Monomer : Initiator (mole %)	100 : 0.05		100 : 0.05		100 : 0.05	
Temperature (ºC) ***and Time*** (hr)	120ºC, 72 hr		120ºC, 72 hr		120ºC, 72 hr	
% yield (purified)	97.5		96.7		97.0	
Physical Appearance (crude)	white solid		white solid		white solid	
Physical Appearance (purified)	white solid		white solid		white solid	
Molecular weight (g $mole^{-1}$)						
$\overline{M}_{n,Theory}$	228,380		228,420		228,810	
GPC						
$\overline{M}_n$	16,970		19,780		16,270	
$\overline{M}_w$	53,680		60,630		60,030	
$\overline{M}_v$	46,640		51,400		50,420	
Dilute-Solution Viscometry						
[η] in THF at 30ºC (dl/g)	0.69		0.74		0.63	
$\overline{M}_v$	47,030		51,851		41,904	
Thermal Properties						
DSC	1st run	2nd run	1st run	2nd run	1st run	2nd run
T_m, onset (ºC)	54.8	53.6	56.0	52.9	51.2	52.6
peak (ºC)	58.8	55.8	61.2	56.7	56.2	55.3
Heat of Fusion (J/g)	80.8	59.8	56.2	57.9	63.5	57.3
Degree of Crystallinity (%)	59.8	44.3	41.6	42.9	47.0	42.4
TGA						
$T_{d,\ 10\%}$ (ºC)	392		389		390	
$T_{d,\ 50\%}$ (ºC)	450		448		451	
$T_{d,\ range}$ (ºC)	178-590		185-563		133-568	
Mechanical Properties						
Tensile Testing						
Stress at Break (MPa)	11.30 ± 1.08		8.59 ± 1.02		10.03 ± 1.10	
Elongation at break (%)	19.76 ± 2.54		22.66 ± 3.21		53.96 ± 2.82	
Young's Modulus (MPa)	252.46 ± 36.34		220.07 ± 25.78		215.27 ± 13.20	

3.3.1 Molecular Weight Determinations of High Molecular Weight PCL by GPC and Dilute-Solution Viscometry

The molecular weights ($\overline{M}_n$, $\overline{M}_w$ and $\overline{M}_v$) were determined by GPC as shown in Table 3.5. The theoretical molecular weights of terpolymers ($M_{n,cal} \approx$ 228,000) can be predicted based on the molar ratio of monomer to initiator practically participating in the polymerization. It was found that the $\overline{M}_n$'s values of all PCLs from GPC results ($\overline{M}_n \approx$ 16,000-19,000) are lower than the theoretical value. This may be ascribed to another hydroxyl initiation (water and hydroxyl-containing impurities in the system) or transesterification reaction may be occurred. It also believed that the molecular weight can be controlled by the monomer to initiator ratio within a limited range. However, the PCL_PTOL showed higher molecular weight than PCL_1-hexanol and PCL_macroinitiator because of the difficult dissolving of the PTOL initiator in cyclic esters monomers lead to lower PTOL concentration.

The intrinsic viscosity [η] values of the PCLs were obtained from their reduced and inherent viscosity-concentration plots. The results obtained for determining [η] and $\overline{M}_v$ by Mark-Houwink Sakurada equations are summarized in Table 3.5. It was found that in dilute solution, star-shaped PCL_macroinitiator lower intrinsic viscosity than linear PCL at the same molecular weight ($\overline{M}_n$), indicating the expected star-shaped structure. This is due to the fact that intrinsic viscosity reflects the chain conformation of the polymer in dilute solution.

3.3.2 Thermal Characterization of High Molecular Weight PCL by DSC

Thermal analysis of the high molecular weight linear and star-shaped PCLs was carried out by means of DSC. To enable them to be compared, all of the PCLs samples had the same thermal histories. DSC analyses were conducted at the heating rate of 10ºC/min under dry nitrogen atmosphere. The DSC thermograms for both first and second hating runs are shown in Figures 3.13-3.14 and thermal properties results are compared in Table 3.5.

DSC curves of linear and star-shaped PCLs have a single melting peak both in first and second heating run. Normally, the thermal properties will affected when branching points are introduced into the polymer and influences T_m and crystallinity. The imperfect crystallization possibly existed in the star-shaped PCLs but not in the linear PCL which rearrange and crystallize easily. However, the melting temperatures (T_m) and degree of crystallinity of star-shaped PCLs (PCL_PTOL and PCL_maroinitiator) are slighly lower than that of linear (PCL_1-hexanol) in this study. The results seem to suggest that the crystallization rearrangement of polymer chain ends is interrupted by the highly branched architecture of these polymers.

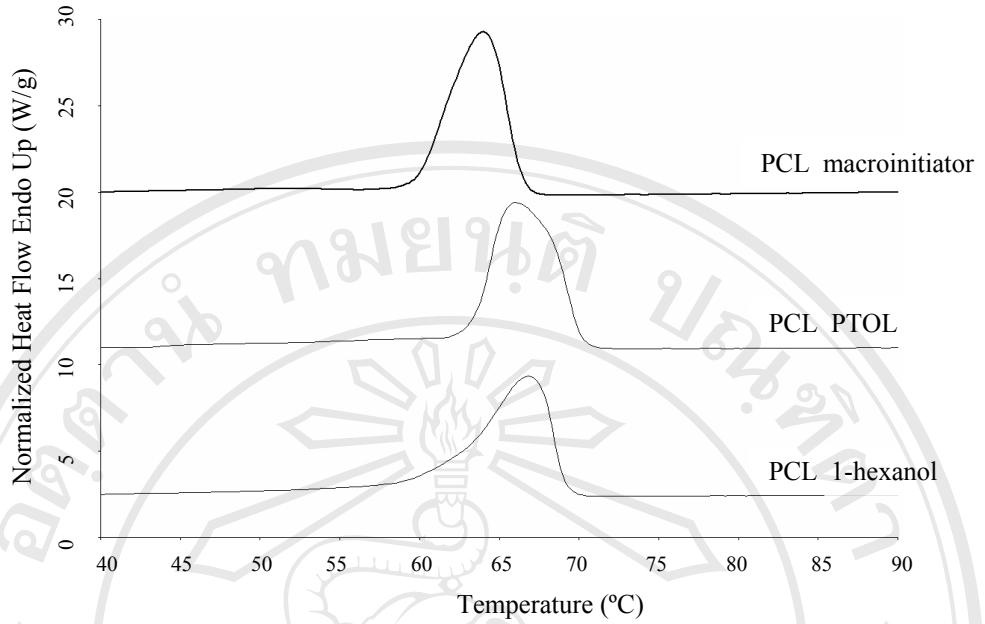

Figure 3.13 Comparison of the DSC thermograms first run of linear and star-shaped high molecular weight poly(*ε*-caprolactone) homopolymers.

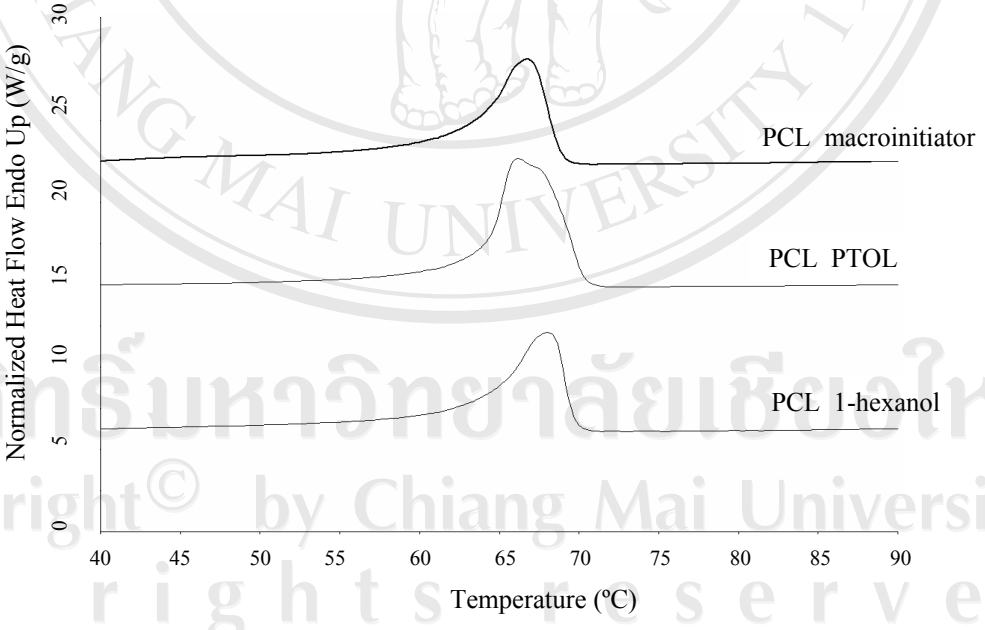

Figure 3.14 Comparison of the DSC thermograms second run of linear and star-shaped high molecular weight poly(*ε*-caprolactone) homopolymers.

3.3.3 Thermal Characterization of High Molecular Weight PCL by TG

The TG thermograms and thermal degradation ranges of the linear and star-shaped high molecular weight PCLs are compared in Figure 3.15 and Table 3.5. From TG thermograms, the star-shaped PCLs start to decompose at lower temperature than linear PCL. Although TG is not a particularly informative technique as far as polymer characterization is concerned, it is extremely useful when combined with DSC data for defining the melt processing range of polymers. In this study, the star-shaped PCLs can be processed at lower temperature than their linear counterparts because lower T_m and lower T_d, which could be advantageous, especially in the melt processing of thermo-labile polyesters.

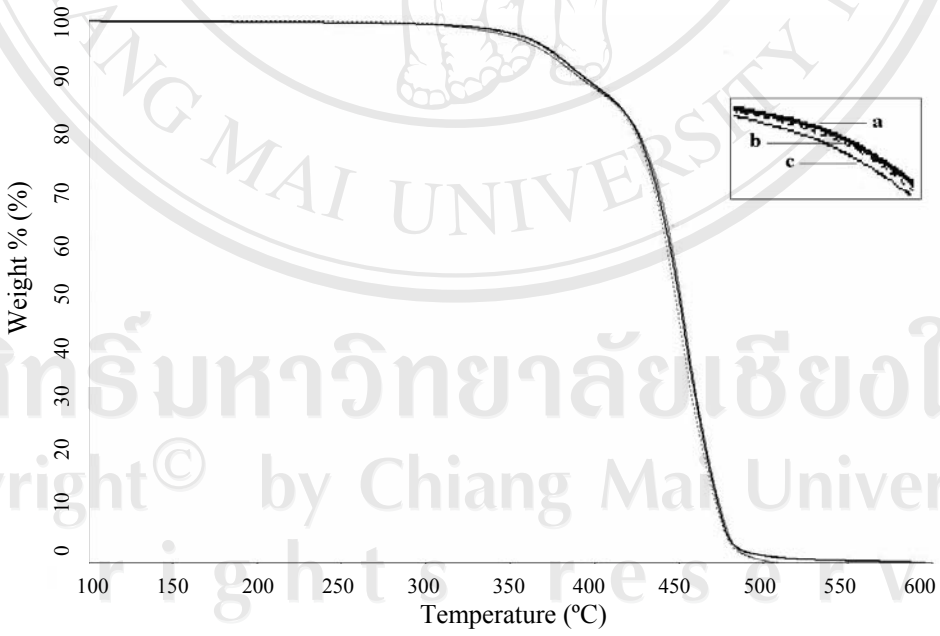

Figure 3.15 Comparison of the TG thermograms of homopolrmers; (a) PCL_1-Hexanol, (b) PCL_PTOL and (C) PCL_macroinitiator.

3.3.4 Mechanical Properties of High Molecular Weight PCL by Tensile Testing

The stress-strain curves of all PCL films are shown in Figure 3.16 and the derived property values (stress at break, % elongation at break and Young's modulus) are compared in Table 3.5. The PCL_macroinitiator showed higher %elongation at break (53%) than PCL_PTOL and PCL_1-hexanol (22% and 19% respectively). These results meant star-shaped PCL were more flexible than linear PCL and could be suggested from these results that molecular architecture of PCL affect the properties.

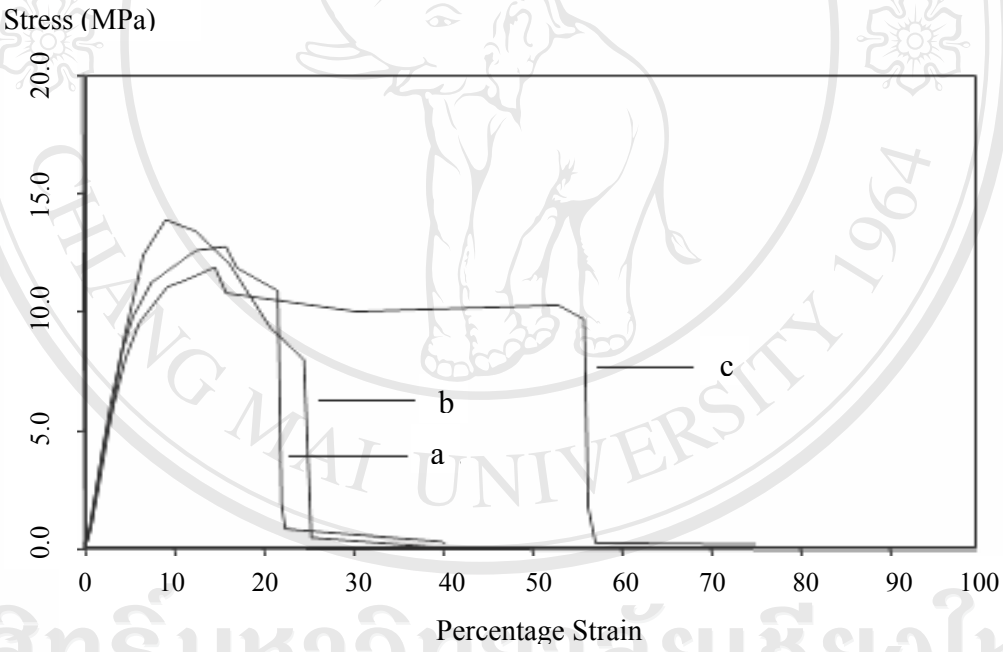

Figure 3.16 Comparison of the stress-strain curve of homopolymer; (a) PCL_1-hexanol, (b) PCL_PTOL and (C) PCL_macroinitiator.

3.3.5 Rheological Properties of High Molecular Weight PCL by Melt Rheology Measurement

One of the best methods to characterize the mechanical properties of polymer melts with respect to structure is melt rheology. The effect of molecular architecture on polymer properties in the melt was investigated in this study. Measurements of zero shear viscosity, η_o were performed as a function of frequency paralleled plate geometry of a Bohlin Gemini HR^{nano} Rotational Rheometer as described in section 2.4.9. The rheological behaviors of all samples were analyzed by shear rate of 0.1 to 100 rad/s under isothermal condition at 80ºC. The η_0 measurements were preformed by measuring viscosity as a function of shear rate.

Figure 3.17 shows η_0, as a function of shear rate for the high molecular weight linear and star-shaped PCL. In principle, shear viscosity of a pure polymer is divided into two distinct regions including the Newtonian and shear thinning regions as could be seen in Figure 3.17. Comparison of the flow curve for the linear and star-shaped PCLs at the same molecular weight, it was found that the η_o of PCL_1-hexanol was higher than PCL_macroinitiator at the low shear rates. It is generally found that the η_o decreases as short chains are added to a polymer backbone. Branching is often introduced to modify the flow properties of polymeric materials for specific forming operations. In contrast, the η_o of linear PCL was lower than star-shaped PCLs at the high shear rates. The expected behavior for a material with long chains is evident and this type of flow behavior is advantageous for certain processing operations.

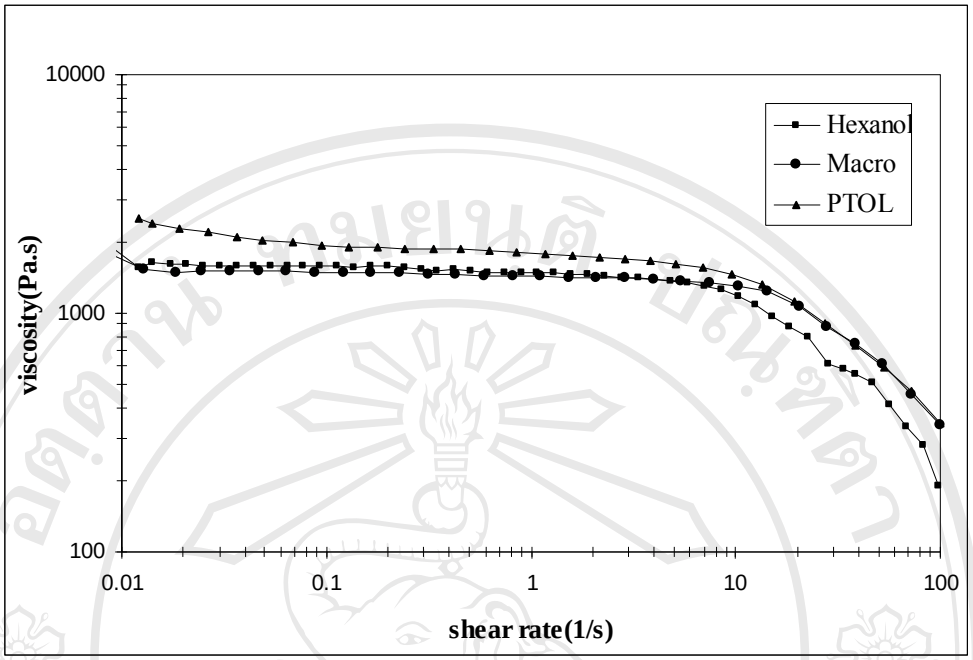

Figure 3.17 The viscosity and stress vs. shear rate (l/s) of linear and star-shaped PCL at 80ºC.

3.4 Synthesis and Characterization of High Molecular Weight PLL with Different Molecular Architectures

The ROP of high molecular weight PLLs homopolymers were prepared using 1 mole % initiator and 0.1 mole% $SnOct_2$ as catalyst at 120ºC for 48 hours. The structure of the polymer depends on the alcohol used. Monofunctional alcohol (1-hexanol) yielded linear PLL (PLL_1-hexanol), while multifunctional alcohols (PTOL) and multifunctional pentaerythritol tetrakis(6'-hydroxyhexanoate) macroinitiator yielded star-shaped PLLs (PLL_PTOL and PLL_macroinitiator respectively) as shown in Figure 3.18 (a-c). The polymer molecular weight was fixed by controlling monomer to hydroxyl group molar ratio.

The properties of the resulting PLLs were characterized as the molecular architecture-properties relationships by combination of techniques: molecular weight determination by dilute-solution viscometry and thermal transition by DSC the results are shown in Table 3.6. Also, the "*in vitro*" hydrolytic biodegradability of the films was studied as an indication of their potential use in biomedical applications.

3.4.1 Molecular Weight Determinations of High Molecular Weight PLL by Dilute-Solution Viscometry

The intrinsic viscosity [η] values of the PLLs were obtained from their reduced and inherent viscosity-concentration plots. The results obtained for determining [η] and $\overline{M}_v$ by Mark-Houwink Sakurada equations are summarized in Table 3.6. From the dilute-solution viscometry results, it was found that star-shaped PLLs exhibited lower [η] and $\overline{M}_v$ than those of linear PLL at same molecular weight ($\overline{M_n}$), supportive of the expected star-shaped structure. This is due to the fact that intrinsic viscosity reflects the chain conformation of the polymer in dilute solution. The star-shaped PLL occupies a smaller hydrodynamic volume in solution than the linear PLL at the same molecular weight.

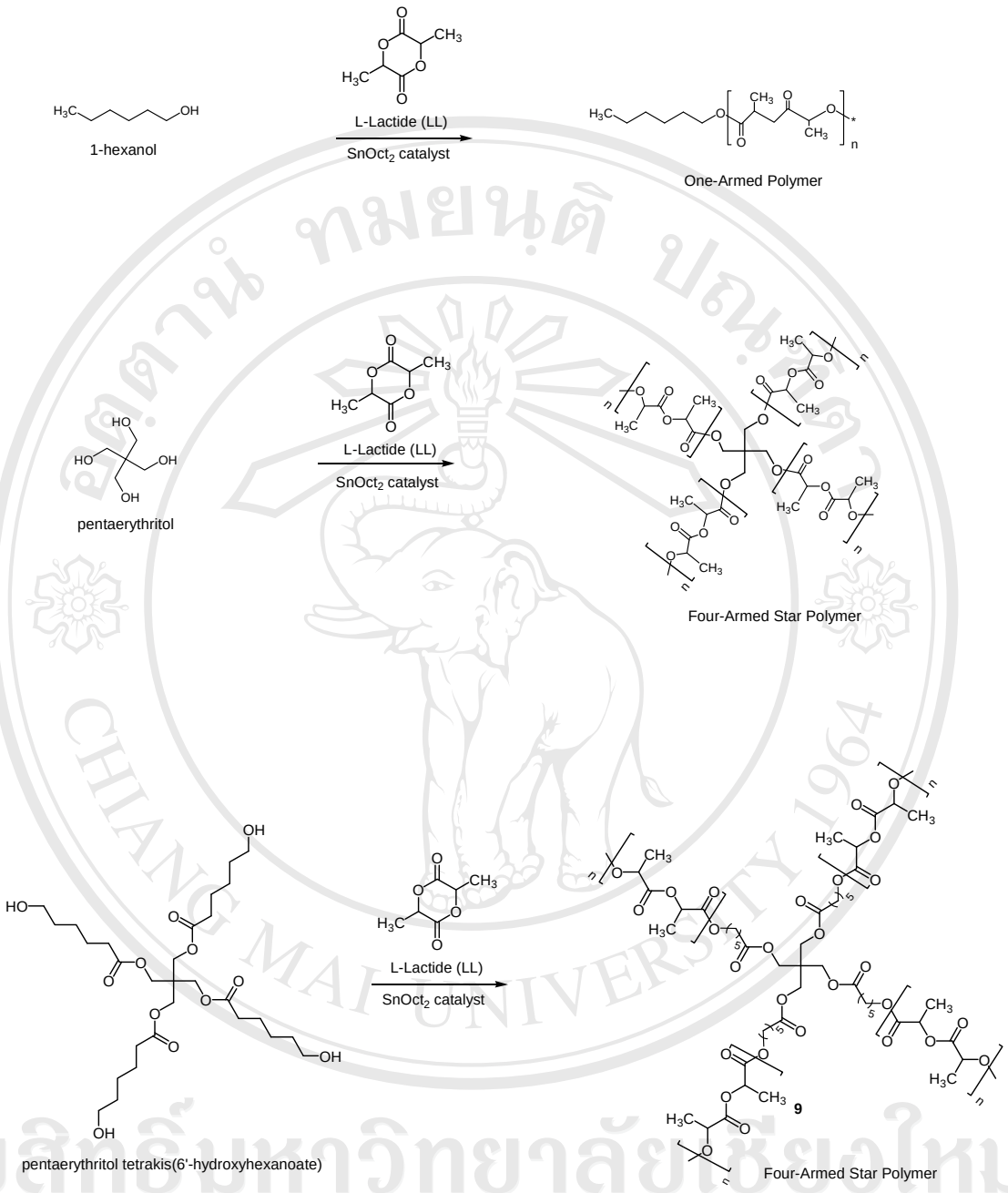

Figure 3.18 Polymerization of L-lactide using (a) 1-hexanol (b) PTOL and (c) pentaerythritol tetrakis(6'-hydroxyhexanoate) as initiators**.**

Table 3.6 The results of high molecular weight PLL homopolymer with different molecular architectures.

Polymer	**PLL_1-hexanol**		**PLL_PTOL**		**PLL_macroinitiator**	
Catalyst (mole %)	$SnOct_2$ (0.1)		$SnOct_2$ (0.1)		$SnOct_2$ (0.1)	
Initiator (mole %)	1-hexanol		PTOL		Macroinitiator	
Monomer : Initiator (mole %)	100 : 1		100 : 1		100 : 1	
Temperature (ºC) ***and Time*** (hr)	120ºC, 48 hr		120ºC, 48 hr		120ºC, 48 hr	
% yield (purified)	94.9		93.4		91.5	
Physical Appearance (crude)	white solid		white solid		white solid	
Physical Appearance (purified)	white solid		white solid		white solid	
Molecular weight (g $mole^{-1}$)						
$\overline{M}_{n,Theory}$	15,114		14,843		15,005	
Dilute-Solution Viscometry						
[η] in $CHCl_3$ at 25ºC (dl/g)	0.42		0.36		0.29	
$\overline{M}_v$	8,925		7,355		5,456	
Thermal Properties						
DSC	1st run	2nd run	1st run	2nd run	1st run	2nd run
T_g (ºC)	-	48.0	-	53.2	-	47.8
T_c, onset (ºC)	100.7	84.4	100.2	100.6	99.6	91.2
peak (ºC)	105.7	88.3	104.7	108.0	102.3	98.7
Heat of Fusion (J/g)	13.1	28.8	5.6	21.9	14.6	13.2
T_m, onset (ºC)	164.5	160.3	153.4	152.4	147.8	149.5
peak (ºC)	170.0	167.3	158.0	157.0	155.3	154.0
Heat of Fusion (J/g)	56.6	52.6	48.0	42.8	45.6	49.7
Degree of Crystallinity (%)	46.5	87.0	57.3	69.1	64.3	67.2

3.4.2 Thermal Characterization of High Molecular Weight PLL by DSC

Thermal properties of linear and star-shaped PLL were characterized by DSC. All samples were measured between 0 to 200ºC at the heating rate of 10ºC/min under dry nitrogen atmosphere. The thermal properties values are shown in Tables 3.6 and DSC thermograms for first and second heating run are compared in Figures 3.19-3.20. The degree of crystallinity (X_c) of PLLs was determined from the enthalpy of melting using the equation (3.6);

$$X_c\,(\%) \;=\; \frac{\Delta H_m \;+\; \Delta H_c}{\Delta H_m{}^{o}} \;\times\; 100 \qquad \text{.....(3.6)}$$

where ΔH_m is the apparent enthalpy of each sample and $\Delta H_m{}^{o}$ is the extrapolated value enthalpy corresponding of a 100% crystalline PLL, 93.6 J/g. ΔH_c is the apparent enthalpy of crystallization of each sample.

The DSC thermograms 1st run as showed that all PLL samples did not exhibit a glass transition (T_g) peak but did show crystallization (T_c) and melting (T_m) peaks. This was due to their thermal histories. In contrast, the DSC thermograms 2nd run all exhibited T_g, T_c and T_m transitions since all samples has been quenched from their melt states. Consequently very little crystallinity was present in the samples prior to the second heating scan. It was found that the T_g of the linear PLL was lower than the star-shaped PLL synthesized from PTOL. This was due to the effect of chain microstructure. The higher T_g of the star-shaped PLL showed that branching hinders segmental motion. It was also observed that the star-shaped PLLs possessed lower

melting points and degrees of crystallinity than the linear PLL, which could be attributed to crystal imperfections mainly due to the short chain lengths of the star-shaped polymers arms. It can also be seen clearly that the T_c of linear PLL is lower than the star-shaped PLLs, attributable to relatively slow crystallization. The globular structures of the star-shaped PLLs decreased the intermolecular interactions and the number of molecular conformations, which facilitated crystallization. Meanwhile, it is noted that the PLLs have two melting peaks resulting from differences in crystallite size and/or shape. These DSC results indicate that the thermal properties and crystallinity are affected when branching point are introduced into the polymer.

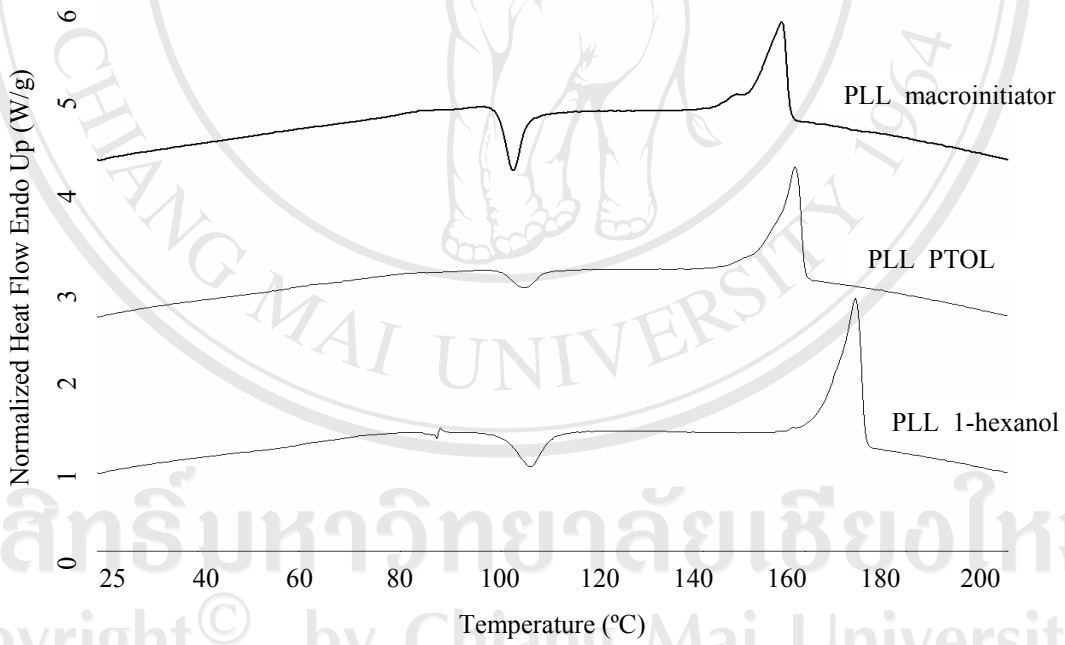

Figure 3.19 Comparison of the DSC thermograms 1st run of the linear and star-shaped PLLs homopolymer.

.

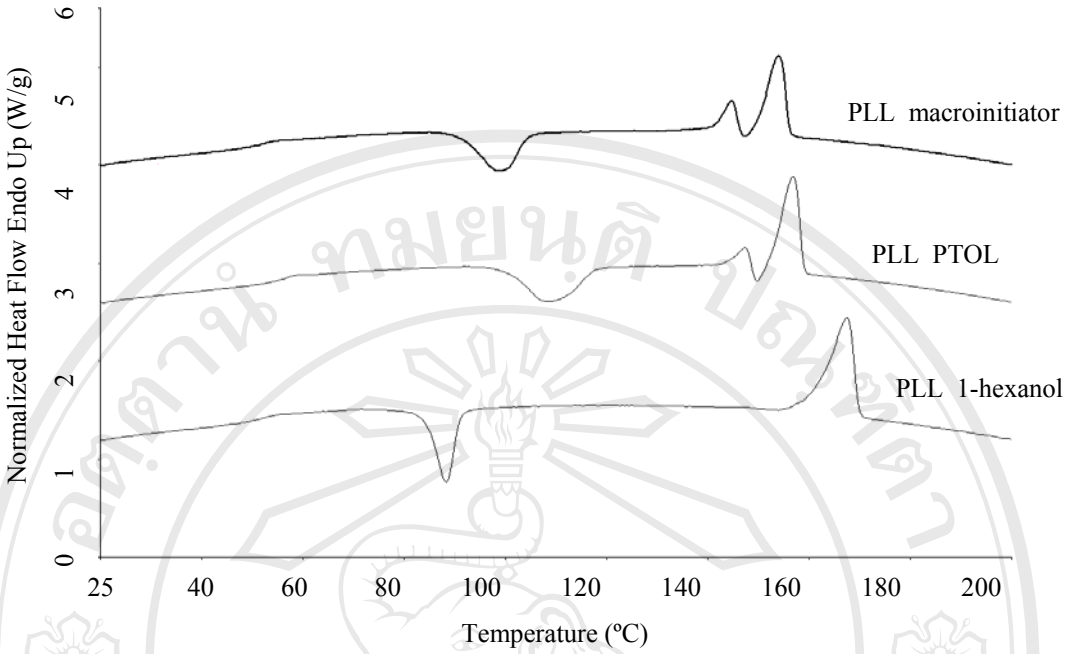

Figure 3.20 Comparison of the DSC thermograms 2nd run of the linear and star-shaped PLLs homopolymer.

.

3.5 *In Vitro* Hydrolytic Biodegradation Studies of High molecular weight PCL and PLL

Linear and star-shaped PCL and PLL films were hydrolyzed in order to study the effects of molecular architectures on the *in vitro* hydrolytic biodegradation. This experiment was selected to provide information about the effect of polymer molecular architecture on the degradation pathway and properties change. The hydrolysis was performed in phosphate buffer saline (PBS) at pH 7.40±0.01 as an immersion medium at body temperature (37±1.0ºC) for 21 weeks. After designated time interval (1, 2, 3, 5, 7, 9, 11, 13, 15, 17 and 21 week), three bottles with different molecular architecture were taken out from the incubator. The film samples were then filtered off, washed carefully with deionized water and dried to constant weight in vacuum oven at room temperature. Normally, the biodegradation of the polymer chain is dependent on the

molecular weight, molecular architecture, % crystallinity and polymer environment [71, 76]. The high molecular weight linear and star-shaped PCLs and PLLs use for *in vitro* hydrolytic degradation study are synthesized and characterized as shown in Tables 3.7 and 3.8 respectively.

Table 3.7 The results of the high molecular weight PCLs with different molecular architectures use for *in vitro* hydrolytic degradation study.

Polymer	PCL_1-hexanol	PCL_PTOL	PCL_macroinitiator
Amount of Polymer (g)	25	25	25
Catalyst (mole%)	$SnOct_2$ (0.1)	$SnOct_2$ (0.1)	$SnOct_2$ (0.1)
Initiator (mole%)	1-hexanol	PTOL	Macroinitiator
Monomer : Initiator (mole%)	100 : 0.005	100 : 0.005	100 : 0.005
Temperature (ºC) ***and Time*** (hr)	120ºC, 72 hr	120ºC, 72 hr	120ºC, 72 hr
% yield (after reprecipitation)	97.0	96.0	97.5
Physical Appearance (crude)	white solid	white solid	white solid
Physical Appearance (purified)	white solid	white solid	white solid
Molecular weight (g mole^{-1})			
GPC			
$\overline{M}_n$	28,400	34,520	31,710
$\overline{M}_w$	89,600	79,730	72,200
$\overline{M}_v$	76,120	79,730	72,200
Dilute-Solution Viscometry			
[η] in THF at 30°C (dl/g)	1.52	1.45	1.42
$\overline{M}_v$	128,493	120,616	117,905

Table 3.8 The results of the high molecular weight PLLs with different molecular architectures use for *in vitro* hydrolytic degradation study.

Polymer	PLL_1-hexanol	PLL_PTOL	PLL_macroinitiator
Amount of monomer (g)	25	25	25
Catalyst (mole%)	$SnOct_2$ (0.1)	$SnOct_2$ (0.1)	$SnOct_2$ (0.1)
Initiator (mole%)	1-hexanol	PTOL	Macroinitiator
Monomer : Initiator (mole%)	100 : 0.005	100 : 0.005	100 : 0.005
Temperature (ºC) ***and Time*** (hr)	120ºC, 72 hr	120ºC, 72 hr	120ºC, 72 hr
% yield (after reprecipitation)	97.5	96.7	97.0
Physical Appearance (crude)	white solid	white solid	white solid
Physical Appearance (purified)	white solid	white solid	white solid
Molecular weight (g $mole^{-1}$) *Dilute-Solution Viscometry*			
$[\eta]$ in $CHCl_3$ at 25ºC (dl/g)	2.84	2.94	2.71
$\overline{M}_v$	123,609	129,307	116,107

The physical appearance of all PCL and PLL films after *in vitro* hydrolytic biodegradation and drying in vacuum oven at room temperature until constant weight was observed. It was found that both linear and star-shaped PCL films were still translucent and flexible during the *in vitro* biodegradation time. In contrast, linear and star-shaped PLL films were transparent and rigid during weeks 1-5 and change from transparent to opaque after week 5. The star-shape PLL_macroinitiator films started to crack in week 15, followed by star-shape PLL_PTOL in week 21.

3.5.1 Weight Loss Profiles

After vacuum drying to constant weight, their % weight retention and % weight loss were calculates as follows:

$$\% \text{ weight retention} = \frac{W_f \times 100}{W_0}$$

$$\% \text{ weight loss} = 100 - \% \text{ weight retention}$$

where W_0 = initial weight of sample and W_f = final weight of sample

The weight, % weight loss, % weight retention and pH of linear and star-shaped PCLs and PLLs immersed in PBS medium at 37±1.0ºC were calculated and recorded as shown in Tables 3.9-3.14.

Table 3.9 Weight, % weight loss, % weight retention and pH of PCL_1-hexanol immersed in PBS medium at 37±1.0ºC.

Time (weeks)	Initial weight ±0.0001g	Final weight ±0.0001g	% weight loss ±0.1%	% weight retention ±0.1%	pH ±0.01
0	0.0157	0.0157	0.0	100.0	7.40
1	0.0140	0.0140	0.0	100.0	7.38
2	0.0136	0.0136	0.0	100.0	7.40
3	0.0142	0.0142	0.0	100.0	7.39
5	0.0144	0.014	0.0	100.0	7.38
7	0.0143	0.0143	0.0	100.0	7.39
9	0.0146	0.0146	0.0	100.0	7.37
11	0.0140	0.0140	0.0	100.0	7.38
13	0.0141	0.0141	0.0	100.0	7.38
15	0.0144	0.0144	0.0	100.0	7.39
17	0.0140	0.0140	0.0	100.0	7.41
21	0.0135	0.0135	0.0	100.0	7.39

Table 3.10 Weight, % weight loss, % weight retention and pH of PCL_PTOL immersed in PBS medium at 37±1.0ºC.

Time (weeks)	Initial weight ±0.0001g	Final weight ±0.0001g	% weight loss ±0.1%	% weight retention ±0.1%	pH ±0.01
0	0.0157	0.0157	0.0	100.0	7.40
1	0.0142	0.0142	0.0	100.0	7.38
2	0.0155	0.0155	0.0	100.0	7.40
3	0.0145	0.0145	0.0	100.0	7.37
5	0.0139	0.0139	0.0	100.0	7.39
7	0.0140	0.0140	0.0	100.0	7.39
9	0.0145	0.0145	0.0	100.0	7.38
11	0.0146	0.0146	0.0	100.0	7.38
13	0.0136	0.0136	0.0	100.0	7.38
15	0.0147	0.0147	0.0	100.0	7.38
17	0.0157	0.0157	0.0	100.0	7.42
21	0.0145	0.0145	0.0	100.0	7.41

Table 3.11 Weight, % weight loss, % weight retention and pH of PCL_macroinitiator immersed in PBS medium at 37±1.0ºC.

Time (weeks)	Initial weight ±0.0001g	Final weight ±0.0001g	% weight loss ±0.1%	% weight retention ±0.1%	pH ±0.01
0	0.0156	0.0156	0.0	100.0	7.40
1	0.0146	0.0146	0.0	100.0	7.36
2	0.0132	0.0132	0.0	100.0	7.40
3	0.0151	0.0151	0.0	100.0	7.40
5	0.0152	0.0152	0.0	100.0	7.37
7	0.0141	0.0141	0.0	100.0	7.40
9	0.0150	0.0150	0.0	100.0	7.39
11	0.0137	0.0137	0.0	100.0	7.38
13	0.0152	0.0152	0.0	100.0	7.39
15	0.0141	0.0141	0.0	100.0	7.37
17	0.0140	0.0140	0.0	100.0	7.41
21	0.0146	0.0146	0.0	100.0	7.38

Table 3.12 Weight, % weight loss, % weight retention and pH of PLL_1-hexanol immersed in PBS medium at 37±1.0ºC.

Time (weeks)	Initial weight ±0.0001g	Final weight ±0.0001g	% weight loss ±0.1%	% weight retention ±0.1%	pH ±0.01
0	0.0149	0.0149	0.0	100.0	7.40
1	0.0157	0.0154	1.0	99.0	7.36
2	0.0151	0.0145	1.7	98.3	7.32
3	0.0139	0.0133	3.1	96.7	7.23
5	0.0143	0.0136	4.2	95.8	7.10
7	0.0145	0.0137	5.2	94.8	7.11
9	0.0164	0.0154	6.1	93.9	6.89
11	0.0154	0.0141	8.1	91.9	6.60
13	0.0167	0.0152	8.6	91.4	6.54
15	0.0157	0.0142	9.8	90.2	6.38
17	0.0142	0.0125	10.7	89.3	6.12
21	0.0154	0.0134	13.2	86.8	5.97

Table 3.13 Weight, % weight loss, % weight retention and pH of PLL_PTOL immersed in PBS medium at 37±1.0ºC.

Time (weeks)	Initial weight ±0.0001g	Final weight ±0.0001g	% weight loss ±0.1%	% weight retention ±0.1%	pH ±0.01
0	0.0165	0.0165	0.0	100.0	7.40
1	0.0155	0.0150	1.9	98.1	7.35
2	0.0154	0.0147	2.9	97.1	7.29
3	0.0156	0.0149	4.2	95.8	7.11
5	0.0172	0.0163	5.4	94.6	7.00
7	0.0164	0.0154	6.4	93.6	6.80
9	0.0152	0.0144	7.7	92.3	6.52
11	0.0164	0.0148	9.1	90.9	6.36
13	0.0169	0.0151	9.6	90.4	6.30
15	0.0163	0.0145	10.0	90.0	6.15
17	0.0157	0.0137	11.8	88.2	5.92
21	0.0155	0.0133	14.6	85.4	5.68

Table 3.14 Weight, % weight loss, % weight retention and pH of PLL_macroinitiator immersed in PBS medium at 37±1.0ºC.

Time (weeks)	Initial weight ±0.0001g	Final weight ±0.0001g	% weight loss ±0.1%	% weight retention ±0.1%	pH ±0.01
0	0.0149	0.0149	0.0	100.0	7.40
1	0.0154	0.0147	2.7	97.3	7.35
2	0.0163	0.0153	3.4	96.6	7.26
3	0.0158	0.0146	5.6	94.4	7.11
5	0.0172	0.0158	6.2	93.2	6.92
7	0.0187	0.0171	7.6	92.4	6.78
9	0.0171	0.0153	10.3	89.7	6.52
11	0.0170	0.0149	12.9	87.1	6.21
13	0.0162	0.0140	13.7	86.3	5.98
15	0.0157	0.0134	14.9	85.1	5.74
17	0.0162	0.0137	16.1	83.9	5.43
21	0.0170	0.0141	18.4	81.6	5.18

The weight, %weight retention and %weight loss of linear and star-shaped PCLs and PLLs are shown in Tables 3.9-3.14. The corresponding %weight loss and %weight retention profiles of linear and star-shaped PLLs are shown in Figures 3.21-3.22.

From the results obtained in Tables 3.9-3.11, all the linear and star-shaped PCL films were not changed weight during *in vitro* biodegradation periods (21 weeks) due to the fact that PCL has a long degradation time (approximately 3 years) with high crystallinity. In contrast, star-shaped PLL showed a faster degradation rate than linear PLL seems to be due to star-shaped polymers have a different entanglement structure and possess a higher density of chain-end than linear chain of comparable molecular weight. This could be affect mechanical properties and degradation behaviors.

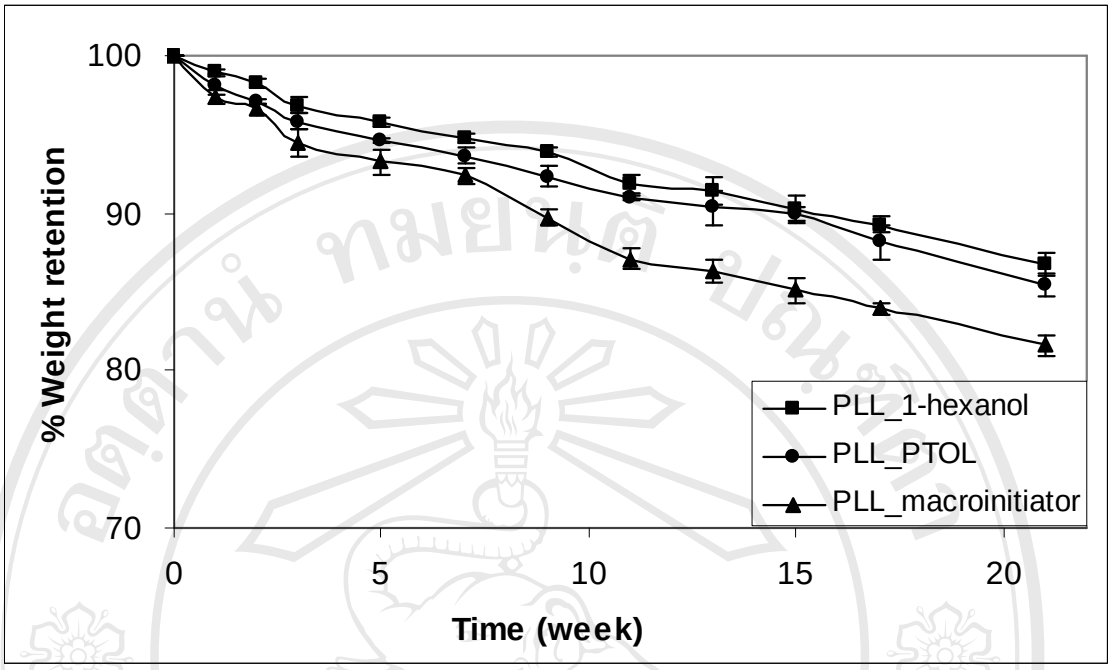

Figure 3.21 Comparison of % weight retention of linear and star-shape PLLs during of the period of the *in vitro* biodegradation experiments.

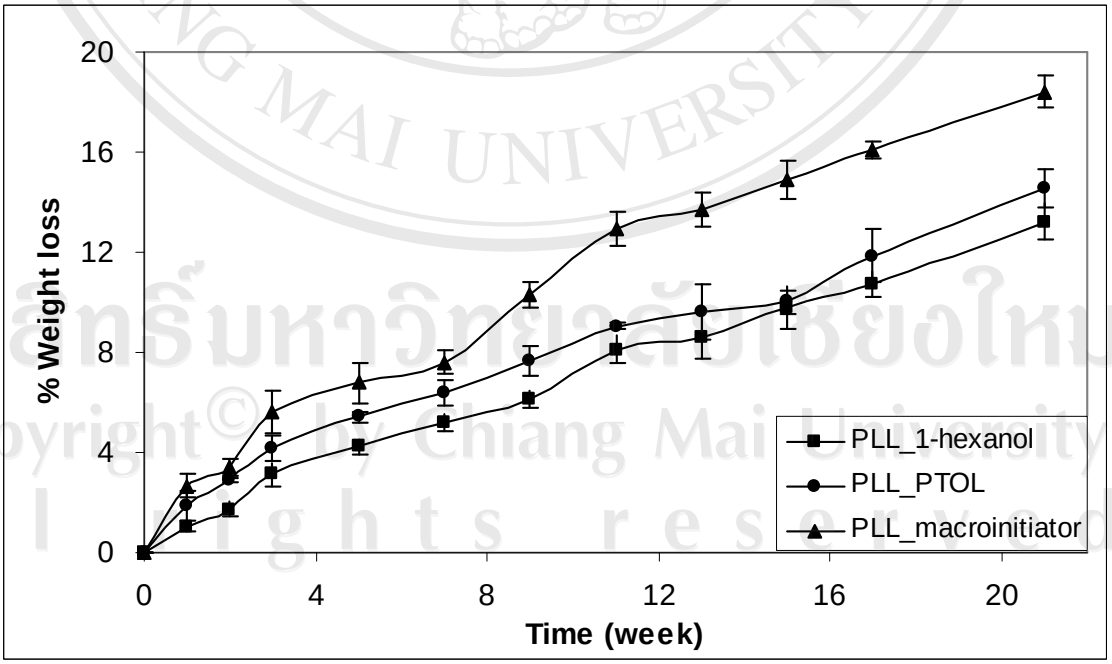

Figure 3.22 Comparison of % weight loss of linear and star-shape PLLs during of the period of the *in vitro* biodegradation experiments.

Although chemical microstructure is the dominant factor for hydrolytic degradation, matrix morphology (% crystallinity and crystallize orientation) is also important. It could be seen that the biodegradation rate of star-shaped PLL_macroinitiator is faster than star-shaped PLL_PTOL, which should be ascribed to the shorter and longer chain in imperfection star-shaped of PLL_PTOL.

The biodegradability of semi-crystalline polymers might be depended on the characteristics of the amorphous region. The proposed degradation proceeds through two main stages: the first stage takes place in the amorphous region; the second in the crystalline region. Within the first stage, because of the molecules in the amorphous region of a polymer are loosely packed, they are more susceptible to attack by solvents than those in the crystalline region and the tie-chain segments in the amorphous regions degrade into fragments. This chain scission results in a lesser degree of entanglement of long-chain molecules located in the amorphous regions. Therefore, the remaining un-degraded chain segments can move and reorganize themselves from a disordered to an order state. Further crystallization is induced and increase in the heat of fusion is thus observed. Therefore, two competing processes hydrolysis and induced crystallization were observed in the hydrolytic degradation. In addition, the weight loss of the polymer samples first occurs in the amorphous regions can lead to an apparent increase in crystallinity that can be confirmed all of star-shaped PLL films were changed into opaque white solid during weeks 15-21. When all of the amorphous regions have been removed by the hydrolysis, the second stage of degradation starts.

For the degradation occurred, the polymer should have hydrolytically unstable functional groups, *e.g.,* ester groups. When these biodegradable polymers

are placed in contact with the physiological environment, water penetrates the polymer matrix and facilitates the hydrolytic chain cleavages, leading to biodegradation. The degradation of these PLLs is believed to be a random chain scission which may take place through hydrolysis in the main chain, side chain or both. Normally, the biodegradability of the polymer chain is dependent on the molecular weight, molecular architecture, % crystallinity and polymer environment. In this experiment all factors were fixed except molecular architectures. From the results obtained, the biodegradation rate of star-shaped PLL_macroinitiator is faster than PLL_PTOL and linear PLL. The higher degradation rate of star-shaped PLLs seems to be due to the higher density of chain-end compared with linear PLL.

3.5.2 pH Stability of Phosphate Immersion Medium

The pH of PBS immersion medium was monitored throughout the period of the experiment. No attempt was made to re-adjust the pH to 7.40 since it was of interest to note how the pH changed. It was found that the initially adjusted pH of 7.40 decreased with time, as showed in Tables 3.9-3.14 and Figure 3.23. The simple hydrolysis reaction can be acid-catalyzed in the event that the new carboxylic acid end groups formed causes the pH of the medium to drop below 7. When these generated groups act as a catalyst, the hydrolytic degradation is called an autocatalytic process.

From the pH profile, two phases can be observed in this plot. In the first phase, the pH of the immersion medium decreased slowly due to the most acid degradation products was tapped inside the polymer matrix. In the second phase, the

pH decreases dramatically because the tapped acid degradation products are released. Normally, the third phase may be occurred in the longer times.

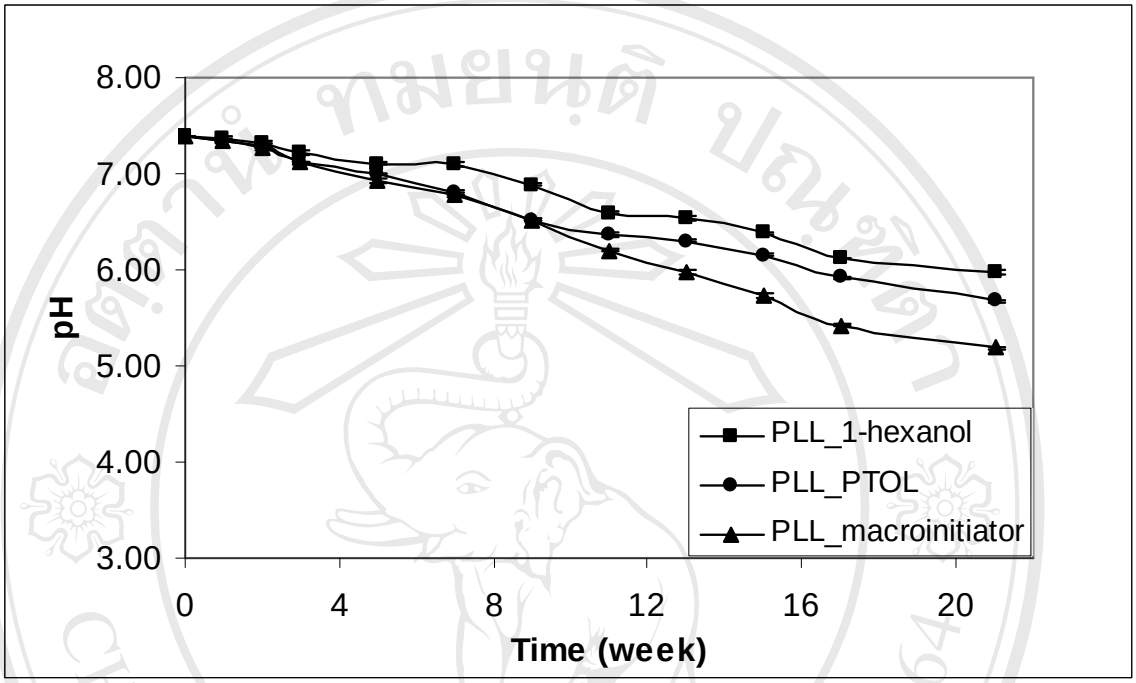

Figure 3.23 Comparison of pH of linear and star-shape PLL during of the period of the in vitro biodegradation experiments.

The star-shaped PLLs were decreased of pH values than linear PLL because of star-shaped had more chain ends and short chain length due to disordered polymer chains and less chain entanglements. The hydrolysis continued inside the hydrated polymer matrix so that the molecular weight of the polymer continuously decreases. Also linear polymer chain can rearrange itself from a disordered to an order state and gave higher crystallinity and strength. The degradation prefers occur in amorphous region more than crystalline region due to water molecules can penetrate easy in amorphous region. From this reason, star-shaped PLL films degraded faster than linear PLL film.

3.5.3 Morphology Determination by DSC

Thermal characterization of linear and star-shaped PLLs immersed in PBS medium at 37±1.0ºC was accomplished by DSC. All samples were measured between 0 to 200ºC at the heating rate of 10ºC/min under dry nitrogen atmosphere. The thermal properties values are shown in Tables 3.15-3.20 and DSC thermograms for first and second heating run are compared in Figures 3.24-3.29.

From DSC data first and second run, all PLL samples possess T_g, T_c and T_m. The degree of crystallinity (X_c) of PLLs was determined from the enthalpy of melting using the equation 3.6. For the results obtained, the % crystallinity of all linear and star-shaped PLL films increased during 1-21 weeks indicated to the molecules in the amorphous region of a polymer were crystallized slowly in immersion medium. The degradation time in weeks 1-21, % crystallinity of star-shaped PLLs are all lower than that linear due to the amorphous region of star-shape PLL is higher. The increasing in amorphous with branching is attributed to shorter chain length and the increase in the number of free chain end, which probably disrupts the orderly fold pattern of the crystal. [77]

DSC thermograms 1st run as showed that all PLL samples did not exhibit a T_c but did show melting (T_m) peaks. This was due to their thermal histories. DSC curves second heating run for linear and star-shaped PLL films are shown in Figures 3.27-3.29. It was found that the T_c and T_m of all PLL films increased during 1-5 weeks, while in weeks 7-21 the T_c and T_m decreased. Earliest stage of *in vitro* biodegradation, the low degradation rate of these PLLs occurred with the molecules in the amorphous region were crystallized at the same time. As the time increase, the

degradation rate increased, which also could be attributed to water penetrates the polymer matrix and facilitates the hydrolytic chain cleavages.

The double melting peaks were observed for the hydrolyzed polymer films, suggesting that two kinds of different fine crystal structures existed in PCL as shown in Figures 3.21-3.23 and melting point decreased with the decrease of crystallite size.

Table 3.15 DSC results for first run of linear PLL_1-hexanol immersed in PBS medium at 37±1.0ºC.

PLL_1-hexanol (week)	DSC (1st run)								
	$T_{g,onset}$ (ºC)	$T_{g,half}$ (ºC)	$T_{c,onset}$ (ºC)	$T_{c,peak}$ (ºC)	ΔH_c (J/g)	$T_{m,onset}$ (ºC)	$T_{m,peak}$ (ºC)	ΔH_m (J/g)	X_c (%)
0	-	-	-	-	-	148.0	157.2	24.4	26.1
1	-	-	-	-	-	147.5	157.3	23.5	25.1
2	-	-	-	-	-	152.9	161.5	27.8	29.7
3	-	-	-	-	-	153.8	161.67	25.6	27.4
5	-	-	-	-	-	151.9	161.7	26.6	28.5
7	42.0	47.5	-	-	-	153.2	164.0	35.0	37.4
9	-	-	-	-	-	151.4	165.0	22.5	24.0
11	48.0	50.2	-	-	-	156.4	165.0	41.3	44.2
13	45.8	49.6	-	-	-	156.8	162.8	39.5	42.2
15	-	-	-	-	-	159.0	163.2	39.7	42.4
17	-	-	-	-	-	158.0	164.7	37.8	40.4
21	-	-	-	-	-	156.8	162.2	40.9	43.7

Table 3.16 DSC results for second run of linear PLL_1-hexanol immersed in PBS medium at 37±1.0ºC.

PLL_1-hexanol (week)	DSC (2nd run)								
	$T_{g,}$onset (ºC)	T_g,half (ºC)	$T_{c,}$onset (ºC)	$T_{c,}$peak (ºC)	ΔH_c (J/g)	$T_{m,}$onset (ºC)	$T_{m,}$peak (ºC)	ΔH_m (J/g)	X_c (%)
0	46.7	51.0	108.7	120.8	18.0	150.6	159.0	27.0	48.1
1	49.8	52.6	105.6	120.7	23.9	152.8	160.2	27.6	55.0
2	58.1	60.0	110.5	127.3	27.8	156.4	161.8	26.7	58.2
3	57.4	58.7	110.2	125.8	26.7	156.3	162.0	31.1	61.8
5	49.1	52.9	101.6	115.3	31.9	151.8	158.0	27.1	63.1
7	55.7	58.3	107.1	121.2	35.6	155.9	161.3	35.9	76.4
9	50.9	54.0	105.9	118.2	34.0	154.8	161.0	35.8	74.5
11	49.6	52.4	104.9	116.0	35.1	162.2	166.5	35.5	75.5
13	53.9	56.0	103.7	113.8	37.3	153.5	158.5	36.8	79.2
15	51.7	53.7	100.3	108.5	37.1	159.3	163.7	39.9	82.2
17	56.7	58.6	104.6	112.7	35.7	160.5	164.8	37.8	78.6
21	55.7	57.3	97.0	106.0	37.6	156.9	162.3	38.3	81.0

Table 3.17 DSC results for first run of star-shaped PLL_PTOL immersed in PBS medium at 37±1.0ºC.

PLL_ PTOL (week)	DSC (1st run)								
	$T_{g,}$onset (ºC)	T_g,half (ºC)	$T_{c,}$onset (ºC)	$T_{c,}$peak (ºC)	ΔH_c (J/g)	$T_{m,}$onset (ºC)	$T_{m,}$peak (ºC)	ΔH_m (J/g)	X_c (%)
0	-	-	-	-	-	151.3	161.2	20.8	28.9
1			-	-	-	150.6	160.2	21.1	22.6
2	38.2	43.3	-	-	-	150.5	160.8	23.8	25.4
3	41.6	43.6	-	-	-	150.7	160.2	22.9	24.5
5	-	-	-	-	-	150.1	159.7	18.8	20.0
7	-	-	-	-	-	150.9	162.7	31.0	33.1
9	-	-	-	-	-	154.1	163.5	29.1	31.1
11	49.6	51.6	-	-	-	155.8	163.7	31.2	33.3
13	-	-	-	-	-	151.7	162.2	32.6	34.8
15	52.9	55.2	-	-	-	158.1	164.3	30.0	32.1
17	54.1	56.7	-	-	-	159.0	164.2	32.7	35.0
21	52.9	55.7	-	-	-	159.4	165.2	34.1	36.4

Table 3.18 DSC results for second run of star-shaped PLL_PTOL immersed in PBS medium at 37±1.0ºC.

PLL_PTOL (week)	DSC (2nd run)								
	T_g,onset (ºC)	T_g,half (ºC)	T_c,onset (ºC)	T_c,peak (ºC)	ΔH_c (J/g)	T_m,onset (ºC)	T_m,peak (ºC)	ΔH_m (J/g)	X_c (%)
0	58.9	61.7	118.1	131.2	8.1	155.6	162.5	15.8	25.5
1	60.2	62.2	113.4	130.8	17.5	154.9	161.0	18.6	38.5
2	57.4	59.8	112.8	129.5	16.5	155.3	161.5	19.9	38.9
3	56.2	58.3	111.2	127.3	19.6	155.0	161.7	24.4	46.9
5	45.2	46.1	101.7	118.3	31.7	151.8	158.7	23.3	58.8
7	56.5	58.7	110.3	125.5	28.1	156.4	161.8	28.5	60.5
9	51.1	53.7	109.5	123.8	28.6	156.2	162.3	30.2	62.8
11	50.6	53.8	107.7	121.8	32.0	155.9	161.5	31.0	66.3
13	53.8	55.7	105.2	120.2	36.8	154.4	159.8	34.8	76.5
15	59.7	61.5	108.3	122.7	36.6	155.9	161.0	34.2	75.6
17	59.6	61.5	108.3	121.2	37.1	156.0	160.8	35.9	78.0
21	58.9	60.9	107.1	116.8	33.1	155.3	159.7	35.5	73.4

Table 3.19 DSC results for first run of star-shaped PLL_macroinitiator immersed in PBS medium at 37±1.0ºC.

PLL_macro initiator (week)	DSC (1st run)								
	T_g,onset (ºC)	T_g,half (ºC)	T_c,onset (ºC)	T_c,peak (ºC)	ΔH_c (J/g)	T_m,onset (ºC)	T_m,peak (ºC)	ΔH_m (J/g)	X_c (%)
0	-	-	-	-	-	147.7	158.8	21.0	22.5
1	-	-	-	-	-	147.9	157.7	24.2	25.8
2	42.4	45.7	-	-	-	156.9	163.8	22.1	23.6
3	47.2	46.8	-	-	-	156.2	163.5	23.5	25.1
5	-	-	-	-	-	153.8	161.3	23.5	25.2
7	42.4	45.9	-	-	-	158.3	164.2	28.6	30.5
9	49.3	51.3	-	-	-	158.5	165.2	31.7	33.8
11	-	-	-	-	-	159.1	164.5	30.5	32.6
13	44.5	48.5	-	-	-	157.5	162.5	33.2	35.4
15	-	-	-	-	-	159.5	164.3	31.9	34.1
17	52.7	54.7	-	-	-	160.3	164.5	33.0	35.3
21	-	-	-	-	-	159.1	164.3	34.3	36.6

Table 3.20 DSC results for second run of star-shaped PLL_macroinitiator immersed in PBS medium at 37±1.0ºC.

PLL_macro initiator (week)	DSC (2nd run)								
	T_g,onset (ºC)	T_g,half (ºC)	T_c,onset (ºC)	T_c,peak (ºC)	ΔH_c (J/g)	T_m,onset (ºC)	T_m,peak (ºC)	ΔH_m (J/g)	X_c (%)
0	60.4	62.6	112.6	126.2	23.5	155.0	160.5	25.2	52.1
1	46.8	50.2	103.0	116.7	21.9	151.4	158.0	27.8	53.1
2	58.4	60.4	111.4	125.7	25.9	157.2	162.5	29.1	58.7
3	57.8	59.8	110.6	127.2	27.6	157.2	162.7	27.8	59.2
5	45.8	47.1	100.1	113.7	29.7	151.4	158.0	24.6	58.0
7	56.7	58.8	107.9	120.5	32.8	156.4	161.5	33.3	70.6
9	49.8	53.6	107.6	119.5	30.6	156.4	161.3	31.8	66.7
11	47.8	52.5	107.1	118.5	30.5	156.3	161.3	31.9	66.8
13	54.0	56.1	103.9	113.8	33.8	153.5	158.5	36.6	75.2
15	59.6	61.4	107.5	116.5	32.9	155.6	160.0	34.1	71.8
17	59.7	60.7	106.3	113.8	33.7	161.6	166.0	34.2	72.5
21	58.5	60.1	104.7	111.7	37.2	161.3	165.5	36.5	78.7

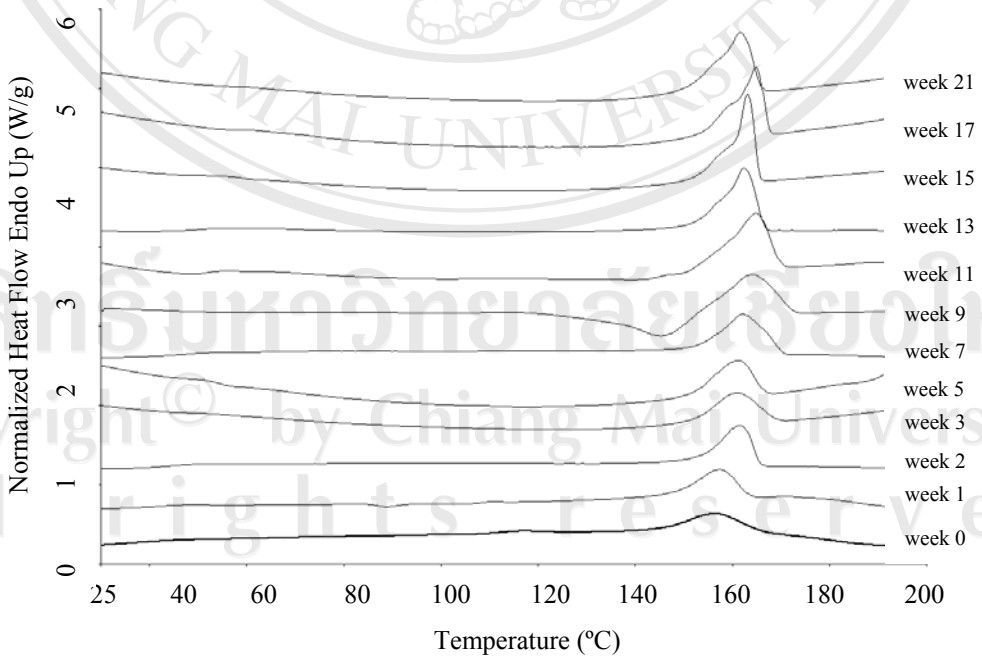

Figure 3.24 Comparison of the DSC thermograms first heating run of PLL_1-hexanol during of the period of the in vitro biodegradation experiments.

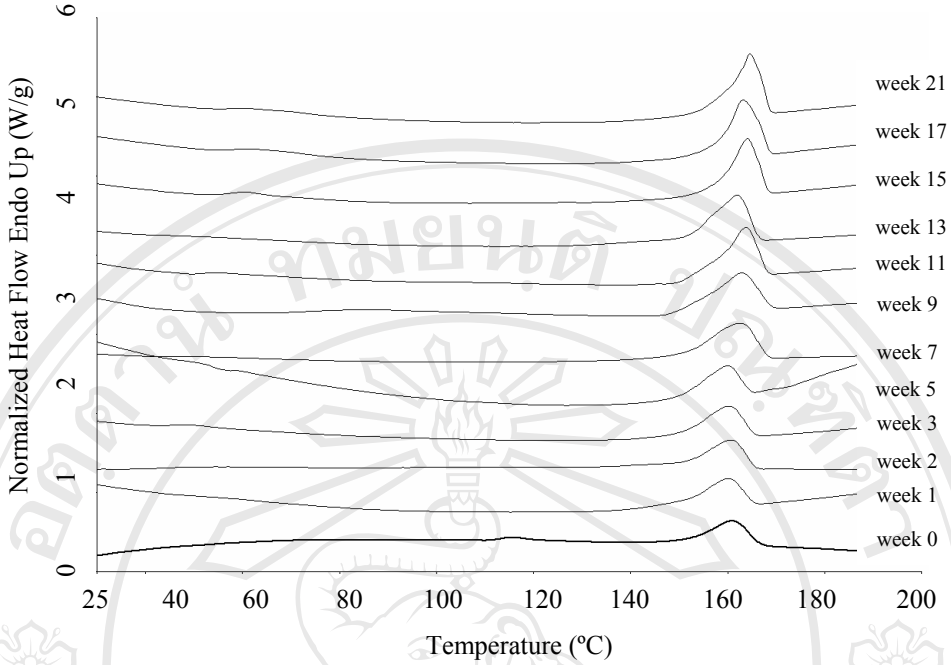

Figure 3.25 Comparison of the DSC thermograms first heating run of PLL_PTOL during of the period of the *in vitro* biodegradation experiments.

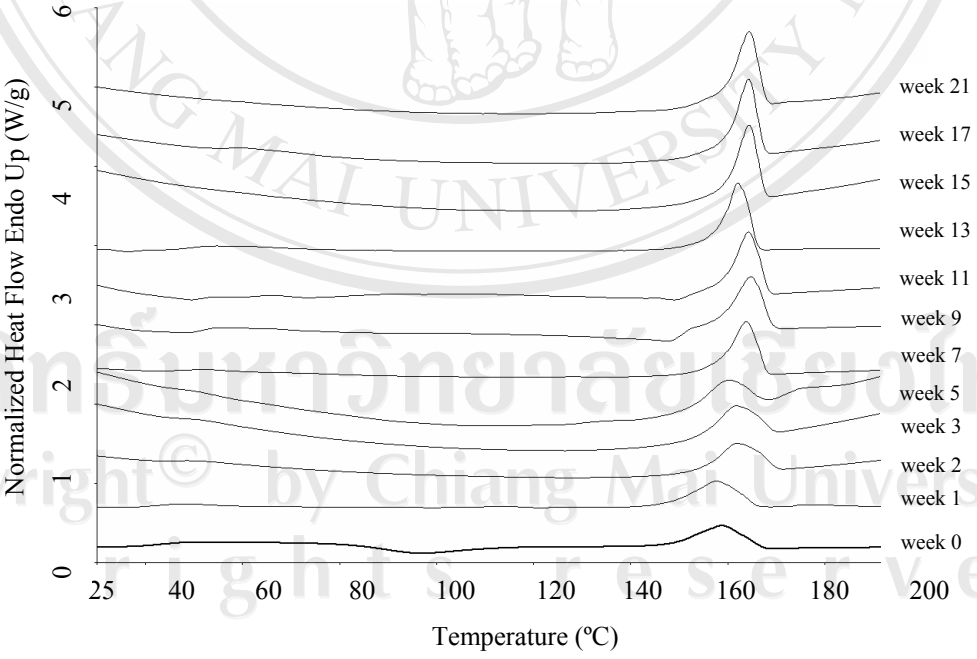

Figure 3.26 Comparison of the DSC thermograms first heating run PLL_macroinitiator during of the period of the *in vitro* biodegradation experiments.

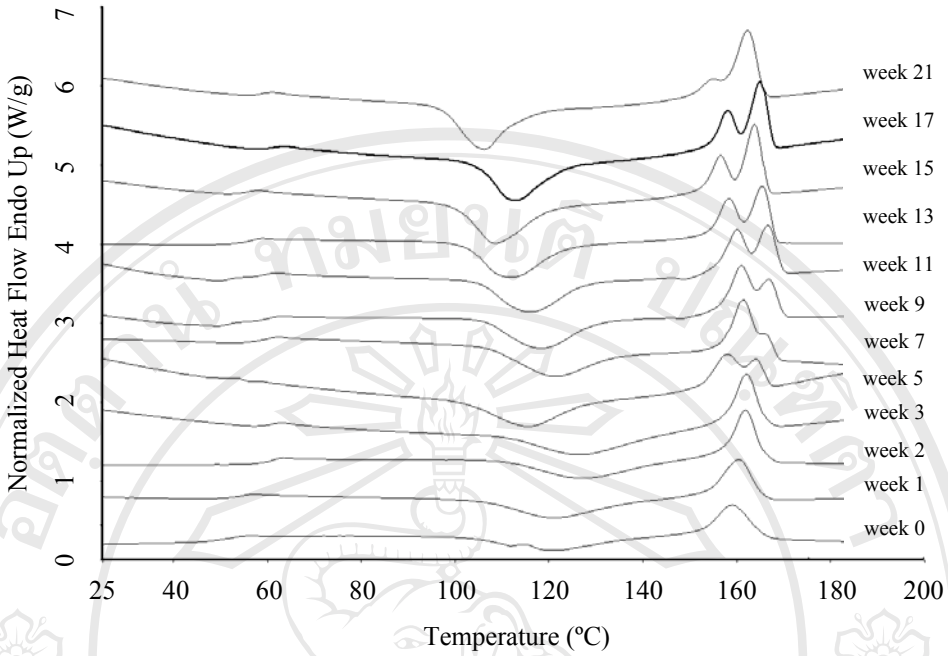

Figure 3.27 Comparison of the DSC thermograms second heating run of PLL_1-hexanol during of the period of the in vitro biodegradation experiments.

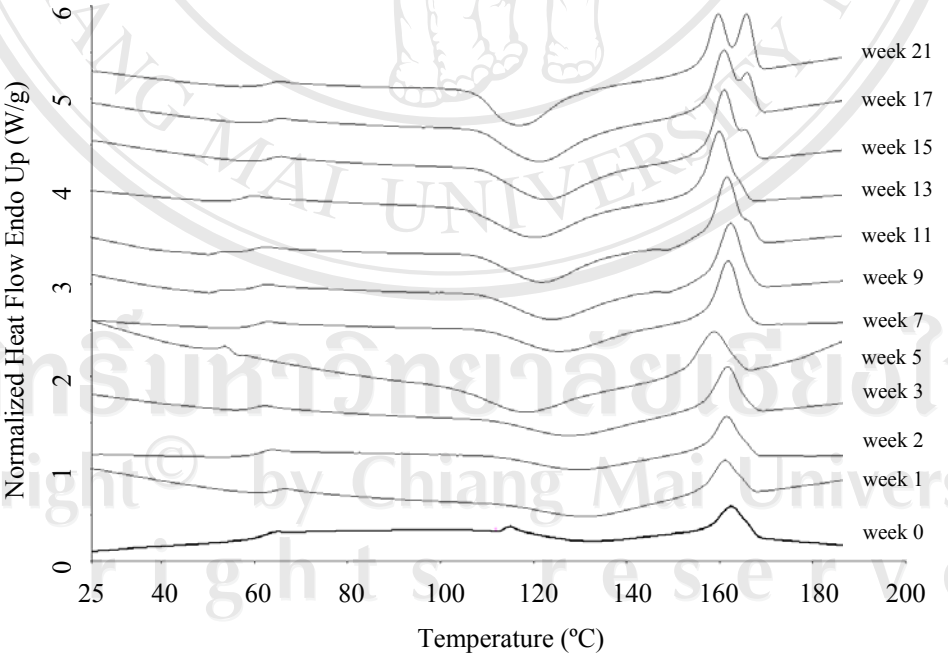

Figure 3.28 Comparison of the DSC thermograms second heating run of PLL_PTOL during of the period of the *in vitro* biodegradation experiments.

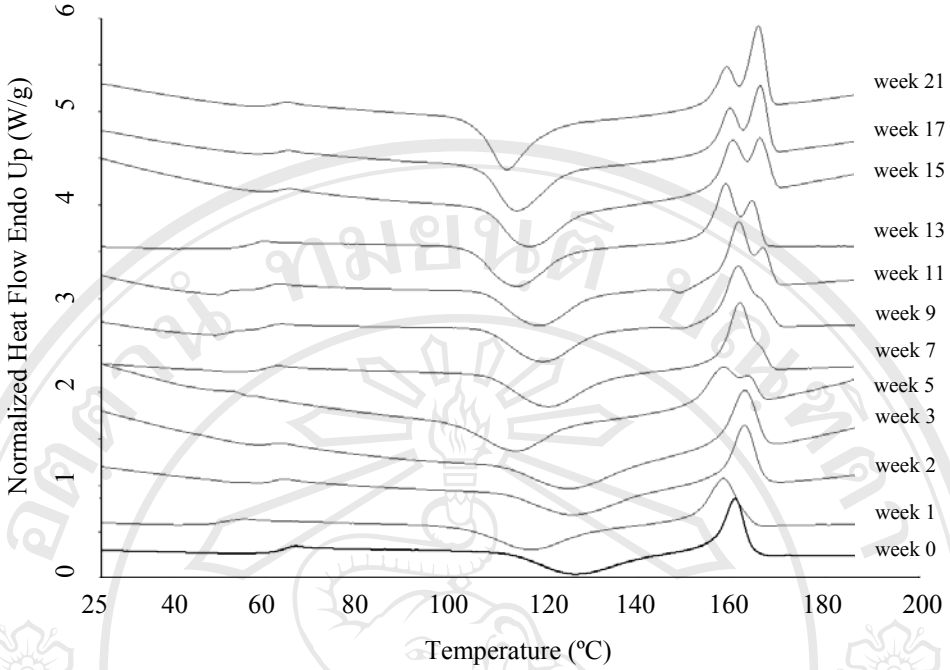

Figure 3.29 Comparison of the DSC thermograms second heating run PLL_macroinitiator during of the period of the *in vitro* biodegradation experiments.

The various stages and processes involved in absorption were described on the following. The first step in hydrolytic degradation process is the absorption of water (hydration) and wetting at the polymer surface. The efficiencies and the rate of these physical processes depend primarily on the hydrophilic and hydrophobic of the polymer and the amount of surface area available for interaction. This is then followed by ester hydrolysis at the surface leading to the formation of micro-defects which facilitate the diffusion of water into the bulk interior of the polymer matrix. The ester hydrolysis occurs preferentially in the amorphous regions where the chains are more loosely packed than in highly-ordered crystalline regions. Then, as hydrolysis precedes the polymer molecular weight decreases until the degradation products are small enough in size to diffuse out the matrix, resulting in mass loss.